The Bentonite Barrier - Swelling Properties, Redox Chemistry and Mineral Evolution

Svensson, Daniel

2015

The Bentonite Barrier

Swelling properties, redox chemistry and mineral evolution

P. Daniel Svensson

DOCTORAL DISSERTATION
by due permission of the Faculty of Engineering, Lund University, Sweden.

To be defended in public at the Center for Chemistry and Chemical Engineering, Lecture Hall K:C, on March 9, 2015, at 13:15.

Faculty opponent

Prof. Jon Otto Fossum, Norwegian University of Science and Technology

Organization

LUND UNIVERSITY

Centre for Analysis and Synthesis, Department of Chemistry, Faculty of Engineering, LTH

PO BOX 124

SE-221 00 LUND, SWEDEN

Author

P. Daniel Svensson

Document name

DOCTORAL DISSERTATION

Date of issue

2015-02-11

Sponsoring organization

Swedish Nuclear Fuel and Waste Management Co (SKB), Oskarshamn, Sweden

Title and subtitle

The Bentonite Barrier - Swelling properties, redox chemistry and mineral evolution

Abstract Bentonite is planned for use as a buffer material in high-level radioactive waste repositories, where safety assessment is performed for very long periods (100-1000 ka). This thesis focuses on the swelling of smectites in liquid water, and analysis of bentonite from field experiments at Äspö Hard Rock Laboratory, Sweden. Four field experiments were analyzed (Alternative Buffer Material experiment, ABM1, ABM2; Temperature Buffer Test, TBT; and Prototype) with focus on Fe- redox chemistry and formation of trioctahedral smectite. The techniques used were mainly synchrotron X-ray diffraction and X-ray absorption spectroscopy. In ABM1 and Prototype the Fe(II)/Fe-total ratio had increased. In TBT no significant increase in Fe(II) was found; instead the corrosion products were dominated by Fe(III). Formation of trioctahedral clays was found in the iron-bentonite experiments (ABM1, ABM2, TBT), but not in Prototype where the heater instead was of copper. In swelling experiments, Ca-Wyoming montmorillonite was shown to expand and partly form a four-water-layer hydrate at lower temperatures in water. This was studied in more detail, and the influence of divalent interlayer cation, temperature, layer charge, salt and irradiation was investigated. Among the investigated smectites, decreased temperature increased the crystalline swelling until ice was formed. Lower smectite layer charge increased the crystalline swelling. Increasing the Gibbs hydration energy of the divalent interlayer cation increased the crystalline swelling. Introduction of salt in the water partly dehydrated the montmorillonite at 20°C, but minimized the dehydration of montmorillonite upon ice formation at low temperatures (-50, -100°C), especially with $CaCl_2$. It was found that in a gradient of ethylene glycol and water a 21 Å basal distance was formed in the montmorillonite, which was higher than in the pure liquids.

Key words: montmorillonite, bentonite, smectite, freezing, thawing, hydration, intercalation, four-water-layer, ethylene glycol, X-ray diffraction, time-resolved, spatial-resolution, XANES, Fe, redox, iron, ABM, TBT, Äspö

Classification system and/or index terms (if any)

Supplementary bibliographical information

Language: English

ISSN and key title

ISBN: 978-91-7422-385-9

Recipient's notes

Number of pages

Price

Security classification

Doctoral Thesis

The Bentonite Barrier

Swelling properties, redox chemistry and mineral evolution

P. Daniel Svensson

Oskarshamn, 2015

Front cover: an example of extensive interaction between corroding iron and bentonite in the ABM2-experiment, very similar to the scraping sample that was examined as a part of this thesis.

Back cover: a bentonite mine at Milos, Greece. Some of the shifts in color are generally interpreted to be due to differences in the iron redox chemistry in the bentonite clay.

Doctoral thesis

All photographs by the author unless otherwise stated

Centre for Analysis and Synthesis,
Department of Chemistry,
Faculty of Engineering, LTH
Lund University

ISBN 978-91-7422-385-9

Printed in Sweden by Media-Tryck, Lund University
Lund 2015

Till Viktoria, William, Linnea,
och mina föräldrar

Populärvetenskaplig sammanfattning på svenska

I Sverige produceras en stor del av elektriciteten i kärnkraftverk och som restprodukt får man ett mycket farligt radioaktivt avfall som måste isoleras från människor i hundratusentals till miljoner år. Svensk Kärnbränslehantering AB (SKB) har i uppdrag att ta hand om detta avfall och har utvecklat metoden KBS-3. I denna placeras det använda kärnbränslet i en kopparkapsel som deponeras på ca 500 meters djup i berget. Mellan kapsel och berg placeras kompakterad bentonitlera som kemiskt och fysiskt skyddar kapseln, och dessutom fördröjer spridningen av eventuella radionuklider om en kapsel skulle gå sönder. Bentonitens svällande egenskaper kommer från dess innehåll av montmorillonit, som vid kontakt med vatten sväller via hydratiseringsprocesser och på det sättet tätar och minskar transporter i kapslens närhet. Avhandlingen är uppdelad i tre områden: (1) montmorilloniters svällning, (2) järnets redoxkemi i bentonit och montmorillonit och (3) bentoniters mineralsammansättning och hur denna kan ändras i fältförsök, med fokus på nybildning av trioktaedriska lermineral. Prover från fyra olika långtidsförsök vid Äspölaboratoriet har använts. Försöken har genomförts nere i berget och i samtliga försök har bentoniten värmts till hög temperatur under lång tid. Mineral- och redox-analyser har gjorts med röntgendiffraktion (XRD) respektive röntgenabsorptions- spektroskopi (XANES) på MAX-labsynkrotronen i Lund.

Svällningsförsöken bidrar till en bättre bild av hur olika montmorilloniter skiljer sig åt och hur externa faktorer som temperatur, salthalt eller motjon kan påverka lermineralets svällande egenskaper. Wyoming-montmorillonit (USA) hade ett annat beteende än montmorillonit från Milos (Grekland) och Kutch (Indien). Detta tolkades bero på montmorilloniternas skillnad i flakladdning, d.v.s. storleken på den negativa laddningen och/eller hur den är fördelad hos mineralflaken.

Järnets redoxkemi i bentoniten från fältförsöken pekar på att mängden återstående syre varit olika i de olika försöken och karaktären på de bildade korrosionsprodukterna har därför också varit olika. I ABM1 hittades syrekänsliga korrosionsprodukter, medan det i TBT fanns maghemit som är en korrosionsprodukt som bildas vid hög temperatur under syrerika förhållanden. I Prototypförsöket observerades en mindre höjning av Fe(II)/Fe(III) kvoten i bentoniten, vilket tolkades som en partiell reduktion av Fe(III) i montmorilloniten, sannolikt som en effekt av den sänkta redoxpotentialen i försöket.

Bentoniternas mineralogiska innehåll efter uppvärmning i fält visade på nybildning av trioktaedriska smektiter i de fall värmaren var av järn. I försöket med koppar kunde inga nya lermineral observeras.

List of papers

The papers are appended at the end of the thesis, with permission from the publishers.

1. **Intercalation of smectite with liquid ethylene glycol - resolved in time and space by synchrotron X-ray diffraction.** P. D. Svensson and S. Hansen (**2010a**) *Applied Clay Science*, **48**, 358-367.

2. **Freezing and thawing of montmorillonite – a time resolved X-ray diffraction study.** P. D. Svensson and S. Hansen (**2010b**) *Applied Clay Science*, **49**, 127-134

3. **Combined salt and temperature impact on montmorillonite hydration** P. D. Svensson and S. Hansen (**2013a**) *Clays and Clay Minerals*, **61**, 328-341.

4. **Redox chemistry in two iron-bentonite field experiments at Äspö Hard Rock Laboratory, Sweden: An XRD and Fe K-edge XANES study.** P. D. Svensson and S. Hansen (**2013b**) *Clays and Clay Minerals,* **61**, 566-579.

5. **Formation of four-water-layer hydrates in smectites with divalent interlayer cations.** P. D. Svensson and S. Hansen (**2014**) *Manuscript*.

Author´s contribution to the included papers:

The author did the major part of the planning, experimental work, evaluation, writing, and all data handling and illustrations.

Additional contributions to publications and reports not included in this thesis

Dohrmann, R., Genske, D., Karnland, O., Kaufhold, S., Kiviranta, L., Olsson, S., Plötze, M., Sandén, T., Sellin, P., **Svensson, D.**, and Valter, M. (2012) Interlaboratory CEC and exchangeable cation study of bentonite buffer materials: I. Cu(II)-triethylentetramine method. ***Clays and Clay Minerals***, 60, 162–175.

Dohrmann, R., Genske, D., Karnland, O., Kaufhold, S., Kiviranta, L., Olsson, S., Plötze, M., Sandén, T., Sellin, P., **Svensson, D.**, and Valter, M. (2012) Interlaboratory CEC and exchangeable cation study of bentonite buffer materials: II. Alternative methods. ***Clays and Clay Minerals***, 60, 176-185.

Kaufhold, S., Dohrmann, R., Sandén, T., Sellin, P., and **Svensson, D.** (2013) Mineralogical investigations of the first package of the alternative buffer material test – I. Alteration of bentonites. ***Clay Minerals***, 48, 199-213.

Kumpulainen, S., Kiviranta, L., Carlsson, T., Muurinen, A., **Svensson, D.**, Sasamoto, H., and Wersin, P. (2010) Long-term alteration of bentonite in the presence of metallic iron. *Swedish Nuclear Fuel and Waste Management Co* (***SKB) Report***, R-10-52.

Olsson, S., Karnland, O., **Svensson, D.**, Lundgren, C. (2013) Chemical and mineralogical characterization of the Indian tunnel backfill bentonite Asha NW BFL-L 2010. *Swedish Nuclear Fuel and Waste Management Co* (***SKB) Report***, TR-13-48.

Olsson, S., Jensen, V. Johannesson, L. E., Hansen, E., Karnland, O., Kumpulainen, K., Kiviranta, L., **Svensson, D.**, Hansen, S., Lindén, J. (2013) Prototype Repository - Hydro-mechanical, chemical and mineralogical characterization of the buffer and tunnel backfill material from the outer section of the Prototype Repository. *Swedish Nuclear Fuel and Waste Management Co* (***SKB) Report***, TR-13-21.

Solano, C., **Svensson, D.**, Olomi, Z., Jensen, J., Wendt, O., Wärnmark, K. (2005) Introduction of aromatic and heteroaromatic groups in the 2- and 8-positions of the Tröger's base core via the Suzuki, Stille and Negishi cross-coupling reactions. A comparative study. **European Journal of Organic Chemistry**, 16, 3510-3517.

Svemar, C., Christiansson, R., Grahm, P., Hagman, P., **Svensson, D.**, Johannesson, L. E., Kristensson, O., Lönnqvist, M., Malmberg, D., Nilsson, U., Wieczorek, K. (2013) Prototype Repository - Opening and retrieval of the outer section of the Prototype. Repository at Äspö Hard Rock Laboratory. Summary Report. *Swedish Nuclear Fuel and Waste Management Co* (***SKB) Report***, TR-13-22.

Svensson, D., Dueck, A., Nilsson, U., Olsson, S., Sandén, T., Eriksson, S., Jägervall, S., and Hansen, S. (2011) Alternative Buffer Material. Status of the ongoing laboratory investigation of reference materials and test package 1. *Swedish Nuclear Fuel and Waste Management Co* (***SKB) Report***, TR-11-06.

Svensson, D., Hansen, S., Bovin, J.-O. (2002) Hurlburtite, the first Be mineral from Västanå iron mine, Skåne, Sweden. **GFF**, 124, 41-43.

Wegdén, M., Kristiansson, P., **Svensson, D.**, Sjöland, A. (2007) The use of focused ion beams for structural characterisation of bentonite. A feasibility study. *Swedish Nuclear Fuel and Waste Management Co* (***SKB) Report***, IPR-09-12.

Oral presentations of parts of the thesis

Svensson, D. (2009) Experiments with smectite resolved in time and space by synchrotron X-ray diffraction. Presentation for Licentiate of Technology degree. October 16, Chemical center, Lund University.

Svensson, D., Hansen, S. (2010) Studying iron redox chemistry in the alternative buffer material experiment using XANES. 4th International meeting, clays in natural & engineered barriers for radioactive waste confinement. March 29-April 1, Nantes, France.

Svensson, D., Hansen, S. (2011) Investigation of iron-bentonite interaction in two large scale field tests in the nuclear waste disposal context. 48th Annual meeting of The Clay Minerals Society, September 24 - 29, Stateline, Nevada, USA.

Svensson, D., Johannesson, L.E., Hansen, S., Sellin, P. (2012) Some synchrotron XRD and XANES results from the excavation of the outer section of the Prototype repository experiment at Äspö hard rock laboratory, Sweden. 49th Annual meeting of The Clay Minerals Society, July 7 – 11, Golden, Colorado, USA.

Svensson, D. (2013) Early observations in a large scale 6½ year iron-bentonite field experiment (ABM2) at Äspö Hard Rock Laboratory, Sweden. 50th Annual meeting of The Clay Minerals Society, October 6–10, Urbana-Champaign, Illinois, USA.

Contents

Introduction

Aims of the work

This thesis studied three areas related to important functions of bentonite for use as a barrier material: (1) the swelling of smectites with liquid water and/or ethylene glycol; (2) Fe redox chemistry in smectites and bentonites; and (3) mineral evolution in bentonite with focus on formation of trioctahedral clay minerals in field experiments at Äspö Hard Rock Laboratory, Oskarshamn, Sweden. The main experimental techniques used were X-ray diffraction and X-ray absorption spectroscopy, which were performed at the MAX-lab synchrotron at Lund University, Sweden.

Bentonite and the repository

Bentonite is planned to be used as a barrier material in repositories for final storage of highly radioactive spent nuclear fuel. The Swedish method for final storage of high level radioactive waste was developed by the Swedish Nuclear Fuel and Waste Management Co (SKB) and is denoted as KBS-3 (**SKB, 2006; SKB, 2011**). In the KBS-3 method (**Figure 1**) the radioactive waste (solid fuel pellets of mainly uraniumdioxide) is to be placed in a copper canister (with a cast iron insert) and sealed by friction stir welding. The copper gives long-term chemical stability and the cast iron gives structural rigidity. The canisters will be placed at a depth of around 500 m in crystalline rock, and the space between the canister and the rock will be filled with specially designed compacted bentonite blocks and pellets.

The most important properties of bentonite in relation to sealing buffers are: (1) high swelling capacity, (2) low hydraulic conductivity, thereby minimizing any mass transport to and from the canister, (3) appropriate plasticity or stiffness as the buffer should keep the canister in position but also be plastic enough so that transfer of any forces from movements in the rock is avoided, (4) adequate long-term stability (in itself and also in combination with various construction materials) and (5) sufficiently high thermal conductivity to ensure rapid heat transfer of the heat generated by the radioactive waste decay. In the case of a broken canister the buffer should also slow down potentially escaping radionuclides by sorption, cation exchange or filtration mechanisms (**Arthur *et al.*, 2005**).

Because of the slow decay, the radioactive waste is considered dangerous for a very long time (100,000 to 1,000,000 years). Therefore, prediction of the long-term safety of the repository requires a highly detailed understanding of the properties of the swelling clay minerals and how these are affected by the surroundings with time.

The tunnels above the deposition holes and inspection boreholes will also be backfilled with bentonite. The huge volume of backfill material introduces challenges regarding how to minimize the cost of the clay in relation to requirements, material logistics and quality control.

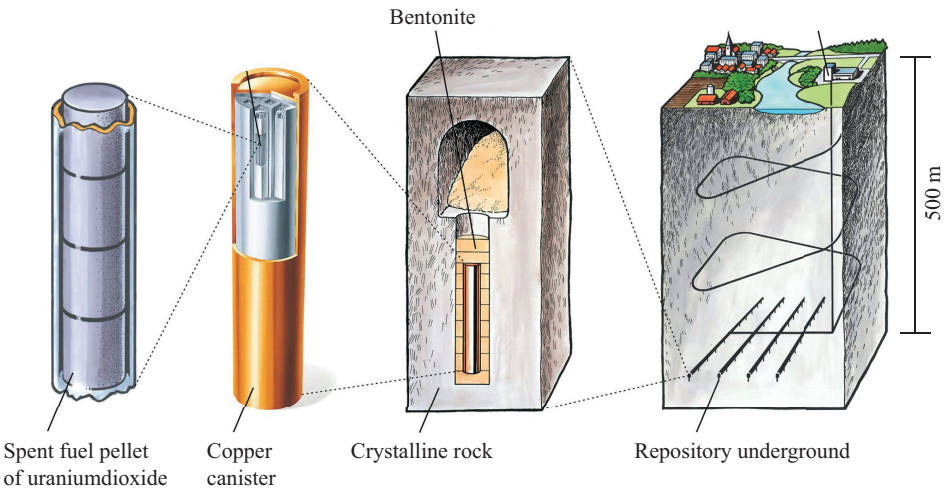

Figure 1. The protective barriers in the KBS-3 method of SKB (copper canister, bentonite clay, and crystalline rock) to keep the radioactive waste isolated from the environment.

Clays, bentonites, and smectites

Bentonite is a swelling clay that consists of swelling clay minerals (smectites), normally montmorillonite, and various accessory minerals. A clay is defined as a naturally occurring material that is composed primarily of fine-grained minerals, which is generally plastic at appropriate water contents and will harden when dried or fired (**Bergaya *et al.* 2006**). A mineral is defined as a naturally occurring (non-manmade) homogeneous solid with a well-defined chemical composition and crystal structure, and is usually formed by inorganic processes (**Klein and Hurlbut 1998**). **Bergaya *et al.* 2006** listed various characteristics of clay minerals, but no stringent or non-ambiguous definition of a clay mineral is given. Clay minerals are genetically either detrital allogenic minerals (transported residues from parent rock with no genetic relation to their present environment) or newly formed secondary or authigenic minerals formed in the sediment where the mineral was found. Smectites are typically authigenic and are often formed by alteration of volcanic rock or by precipitation in alkaline continental basins (**Bergaya *et al.* 2006**). The term bentonite comes from the clay formation at Fort Benton (Wyoming, USA) and bentonite comes in many colors (**Figures 2 and 3**) and qualities. Bentonite is often found in layers with more or less of other layers of sediments on top, and hence in the commercial product, minor contributions from the other layers may also appear sporadically together with various contaminations.

Figure 2. Different colors of bentonite from Bavaria, Germany.

Figure 3. Bentonite in Wyoming, U.S.A. Notice how the color changes in the different parts of the bentonite, which is generally interpreted as being due to differences in the Fe-redox chemistry in the bentonite.

Smectites are layered silicates (phyllosilicates) which are structurally and chemically very similar to the macroscopic mineral mica. Although the difference in chemistry is quite small, the difference in some physical properties, such as swelling, is huge. Stacks of smectite sheets are called tactoids, where each layer is randomly rotated on top of one another; this is called 'turbostratic disorder'.

The smectite layers can be visualized with a transmission electron microscope (**Figures 4 and 5**), and although montmorillonite does not form macroscopic layers which can be seen by the eye, rectorite from Fort Sandeman in Pakistan does, and is perhaps the closest one can come to visually observe montmorillonite layers (**Figure 5**). The Fort Sandeman rectorite is an ordered interstratification (super structure) of a swelling clay mineral (montmorillonite/ beidellite) with a non-swelling clay mineral (illite/mica; **Kodama, 1966**). In dry conditions, this material has a basal reflection (distance between each layer) of 24 Å (14 Å smectite + 10 Å illite/mica), and after liquid water has been added, the smectite component swells, whereas the illite/mica component remains unhydrated, giving the rectorite a basal spacing of 29 Å (19 Å smectite and 10 Å illite/mica; **Svensson, 2014, unpublished results**). Different clay minerals often occur together as interstratified and/or separate phases. An estimation of the amount of illite in an illite-smectite interstratified clay can be made by swelling the sample with ethylene glycol (**Moore and Reynolds, 1997**). Some new details about the contribution of water upon

ethylene glycol swelling were identified in **Svensson and Hansen (2010a)**, which is part of this thesis.

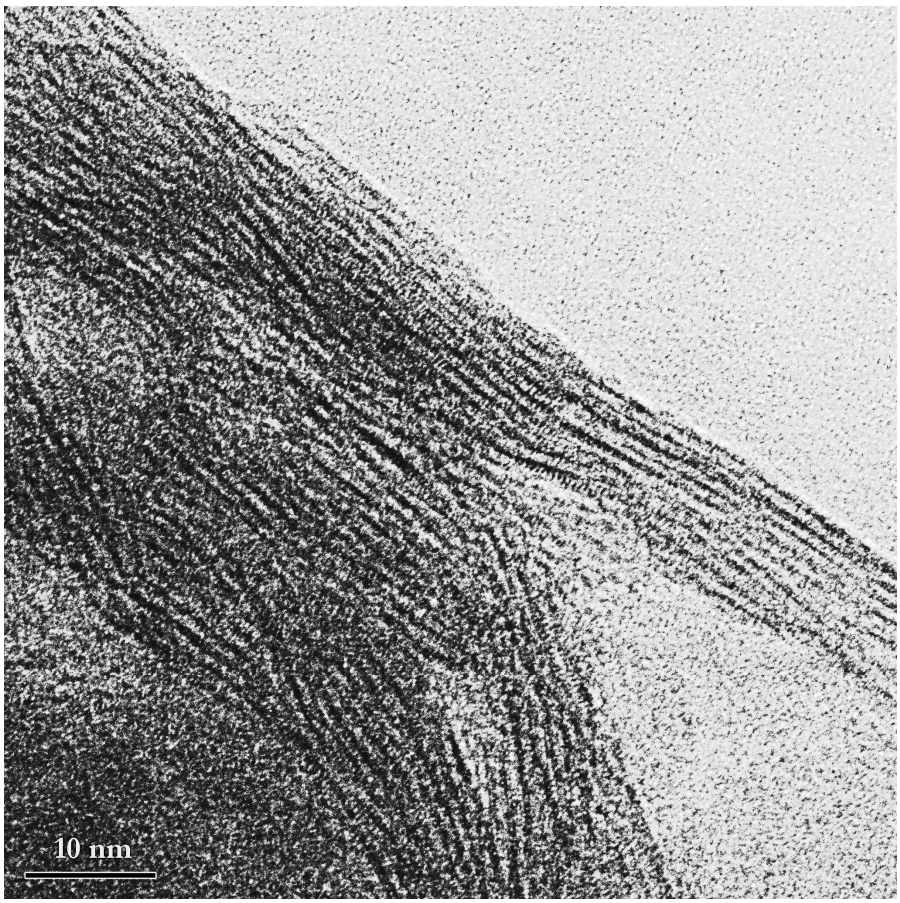

Figure 4. Transmission electron microscopy (TEM) micrograph of Na-montmorillonite (Wyoming) showing a platy texture. The scale bar is 10 nm. Image captured in collaboration with Reine Wallenberg, National Center for High Resolution Electron Microscopy, Lund University.

Figure 5. Left: rectorite from Fort Sandeman, Pakistan. Rectorite is an ordered interstratification of swelling and non-swelling clay minerals (specimen size: 47x35 mm) and is probably the closest one can come to looking macroscopically at montmorillonite. Right: TEM micrograph of Wyoming montmorillonite (image width ≈ 8 μm) showing its platy and wavy structures. Image captured in collaboration with Reine Wallenberg, National Center for High Resolution Electron Microscopy, Lund University.

Clay minerals are divided into 1:1 layer clay minerals with one tetrahedral and one octahedral sheet (*e.g.* kaolinite and serpentine) and 2:1 layer clay minerals, with one octahedral sheet sandwiched between two tetrahedral sheets (*e.g.* pyrophyllite, talc, smectite, vermiculite, and illite; **Figure 6**). In montmorillonite the outer two sheets usually consist of silicon and aluminum (in corner sharing oxygen tetrahedra) and the middle sheet usually contains aluminum, magnesium and iron (in edge sharing oxygen octahedra). Because of isomorphous substitutions in the crystal structure, each 2:1 layer has a negative charge (the most common substitutions are $Al^{3+} \rightarrow Mg^{2+}$ and $Si^{4+} \rightarrow Al^{3+}$). The size of this layer charge is what distinguishes smectites from other phyllosilicate minerals. If the layer charge were larger they would be approaching vermiculites and micas, and if it were absent, they would be pyrophyllite. In order to balance this negative layer charge, positively charged interlayer cations are situated between each layer (**Figure 6c**). The octahedral sheet of the smectite layer can contain three divalent metal ions per half unit cell (*e.g,* Mg^{2+}, Fe^{2+}, Cu^{2+}, Zn^{2+}) and is then called 'trioctahedral', or it can contain two trivalent metal ions (*e.g.*. Al^{3+}, Fe^{3+}, Cr^{3+}) and is then called 'dioctahedral' (**Moore and Reynolds, 1997**). The charge can originate from substitution either in the octahedral layer (*e.g.* dioctahedral montmorillonite and trioctahedral hectorite) or in the tetrahedral layer (*e.g.* dioctahedral beidellite, nontronite and trioctahedral saponite).

An example of a structural formula per unit cell for a sodium saturated Wyoming montmorillonite is:

$Na_{0.65}(Al_{3.1,}\ Mg_{0.49,}\ Fe_{0.38,}\ Ti_{0.01})(Si_{7.89}Al_{0.11})O_{20}(OH)_4$ (**Karnland *et al.* 2006**).

Iron may be present as both Fe(II) and Fe(III) in the octahedral layer and is susceptible to redox reactions. If Fe(III) is reduced to Fe(II) this may impact the layer charge and hence some of the properties of the smectite (**Stucki *et al.* 2002**). The presence of several clay minerals (interstratified or not), accessory minerals, poorly crystallized or amorphous phases and sometimes also organic substances, can make analysis a challenge, especially if the stability of the sample is also taken into consideration.

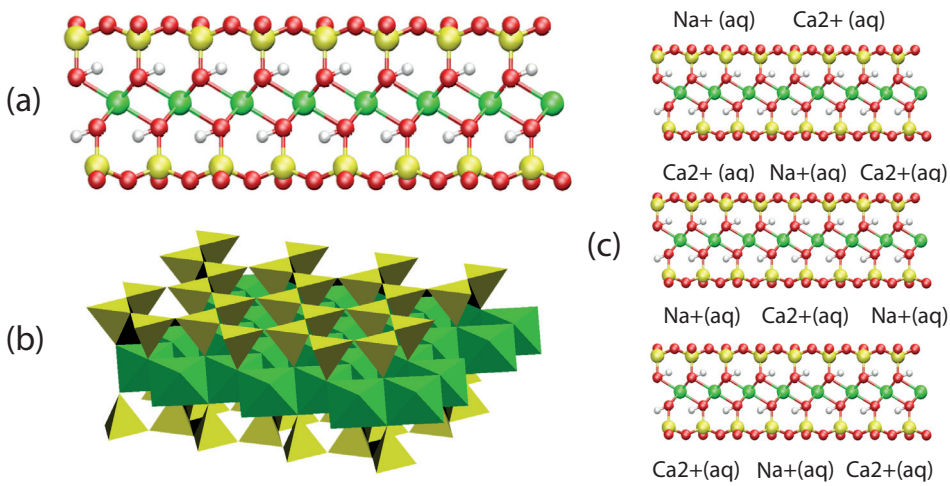

Figure 6. Illustration of the crystal structure of the smectite 2:1 layer. (a) Ball-and-stick representation (green = Al, Mg, Fe; yellow = Si, Al; red = O; white = H). (b) Polyhedral representation. (c) Schematic illustration with interlayer cations in-between the smectite layers. Generated with VMD software by the University of Illinois at Urbana-Champaign, IL, USA.

Experimental

Preparation of pure homoionic smectite

Sodium and calcium montmorillonite swell differently, and in order for a smectite to be dispersed successfully it must contain a certain number of sodium cations in the interlayer. This may be done by cation exchange through repeated washing (3x) using 1 M solutions (0.1 M is enough for divalent cations; **Moore and Reynolds, 1997**). After cation exchange the salt is removed by washing with water followed by dialysis. To separate the clay fraction (*e.g.* < 2 μm particles) sedimentation is used, as large particles sediment faster than smaller ones. This is described by Stoke´s law (**Moore and Reynolds, 1997**):

$$V_T = g\,(d_p - d_l)D^2/18\eta \qquad (1)$$

where V_T is the velocity of sedimentation, g is the force of gravity, d_p-d_l is the difference in density of the particle and the liquid, D is the particle diameter and is the viscosity of the liquid η. The time needed for a specific particle size to sediment to a specific depth can be calculated as $t = h / V_T$, where h is the distance (depth). To speed things up, a centrifuge is normally used. After the separation the clay fraction (*e.g.* < 2 μm diameter size) is obtained.

Cation exchange capacity (CEC)

The specific cation exchange capacity (CEC) of a bentonite depends on the number of cation exchangers in the clay and the specific cation exchange capacity of the smectite itself in terms of charge per gram. If the CEC of the smectite is known, the bulk CEC of a bentonite is a good measure of the smectite content, as long as no other cation exchangers are present. The CEC can be determined in several ways. One method is to extract the cations with an NH_4Cl (or NH_4OAc) solution. Analysis of the extract gives information regarding the type and number of the cations present. One disadvantage with this method is that dissolvable phases (*e.g.* gypsum) also contribute to the result. This can however be minimized with an 80% ethanol solution instead of water (**Belyayeva, 1967**). Another method is to exchange with a Cu^{2+} - triethylenetetramine complex (**Meier and Kahr, 1999**). As the Cu-tri complex has a very strong blue color this reaction can be rapidly

quantified by using spectrophotometry. The exchange reaction is fast and is normally completed in 15- to 30 minutes (**Figure** 7).

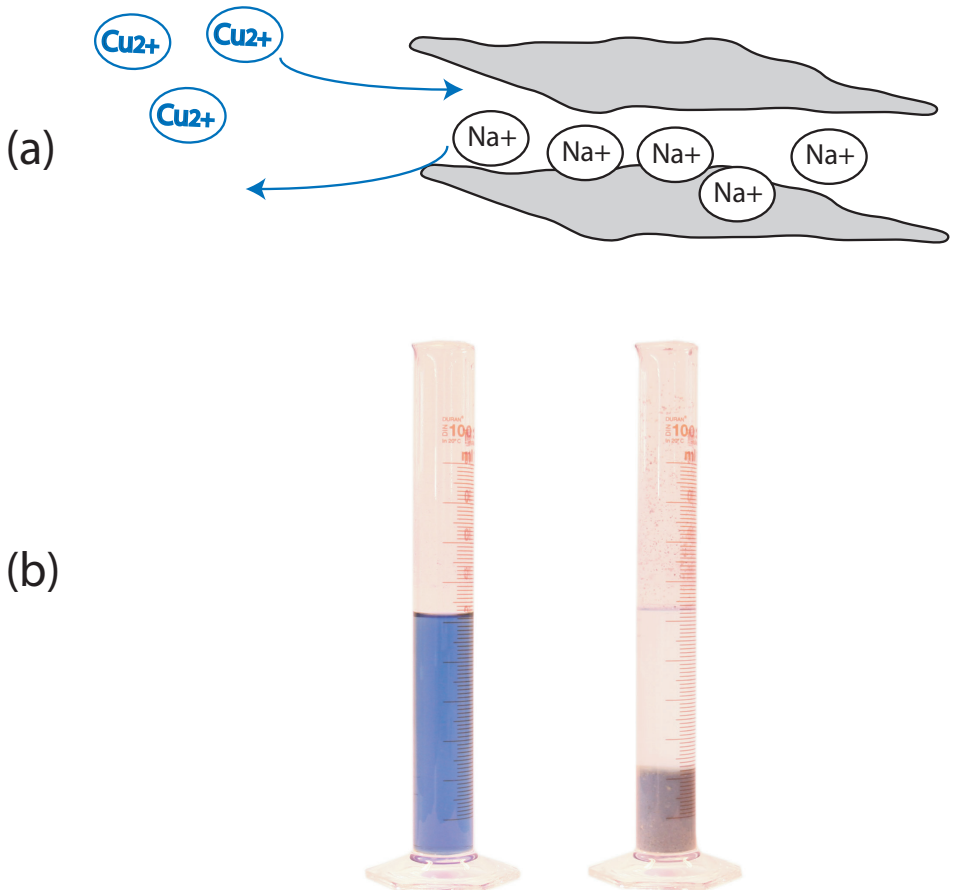

Figure 7. (a) Schematic illustration of the cation exchange reaction of Na^{+} to Cu^{2+} in montmorillonite (b) The cylinder to the left contains a pure solution of a Cu^{2+} complex. In the cylinder to the right, sodium dominated bentonite (MX-80) has been added and mixed with the solution. Decoloring of the solution finished in approximately ten minutes.

Powder X-ray diffraction (XRD)

X-ray diffraction in crystals is called Bragg diffraction and is a consequence of the scattering of coherent X-rays (preferably monochromatic) from the electron clouds surrounding the atoms, and how these scattered photons (waves) interfere with each other through constructive and destructive interference in the crystal structure. Hence, depending on the types of atoms (higher atomic number = more electrons and higher scattering ability) in the structure and their internal geometric relations, different resulting waves will exit the crystal and can be recorded as scattering maxima at different angles in relation to the incident beam. The scattering can be visualized as X-ray scattering from different lattice planes within the crystal structure (**Figure 8**), and the relation between the scattering maxima and interplanar distances is described by Bragg´s law (**Atkins, 1998**):

$$\lambda = 2d_{hkl} \sin \theta_{hkl} \qquad (2)$$

where λ is the wavelength, d is the distance between planes *hkl* giving rise to the diffraction maxima, and θ is half of the angle between the incident and the diffracted beam. A scattering maximum occurs when the X-rays are in phase and constructively interfere with each other. This is the case when the difference in travel path is equivalent to the wavelength, or in other words the distance ABC = λ. The distance AB = d sin θ, and because AB = BC and ABC = 2 AB one can see that ABC = $\lambda = 2d_{hkl} \sin \theta_{hkl}$. For a fixed wavelength, each maximum corresponds to an interplanar distance in the crystal structure. A monochromator can be constructed similarly by keeping the crystal fixed and different wavelengths will thus scatter at different angles which can be separated by a slit. The width of the diffraction peak is a function of the sample particle size and is described by the Scherrer equation (**Patterson, 1939**). Very small particles such as clay minerals give rise to broader peaks, whereas larger crystals give rise to narrower peaks. This is one factor in why clay minerals have broader reflections than most accessory minerals such as quartz, another is the high variability in the composition.

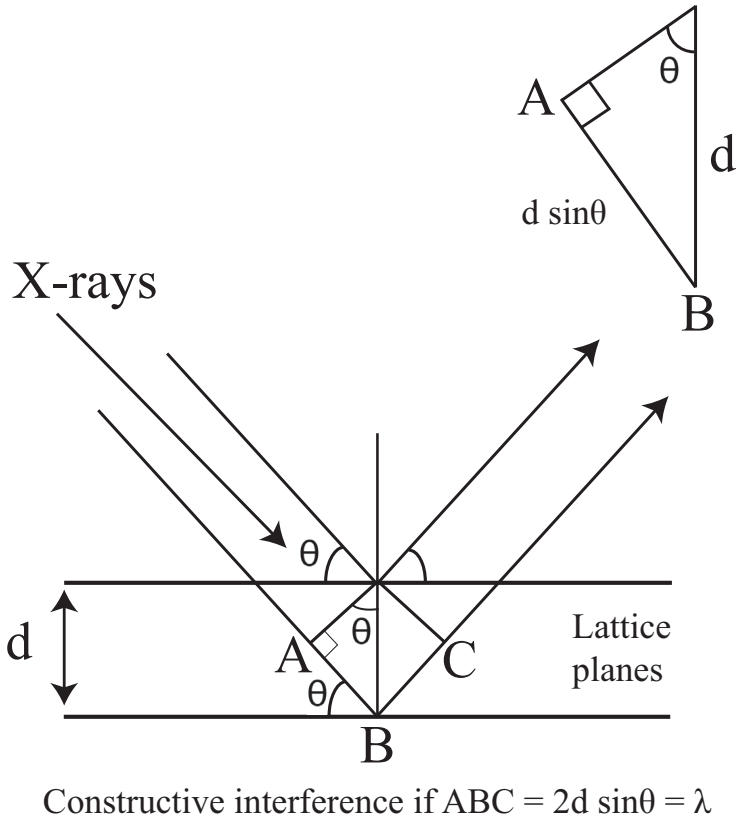

Figure 8. Schematic illustration of Bragg´s law describing X-ray diffraction maxima (λ is the wavelength).

Powder X-ray diffraction - Experimental setup

The beamlines used at MAX-lab, Lund, Sweden were I711 (**Cerenius *et al.*, 2000**) and I911-5 (**Mammen *et al.*, 2002, 2004**). In the experimental hutch the sample holder was attached to the experimental table (**Figure 9**), and the centering of the sample was as perfect as possible, as the distance between the sample and the detector influences the measurement of the scattering angle and hence the calculated d-spacing. Behind the sample a beam stop was situated to protect the detector from high intensity radiation from the direct beam of non-diffracted X-rays. A solid state CCD detector (**Figure 9**) detected the X-ray intensity in a matrix corresponding to a photographic plate. The distance between the sample and the detector was adjusted to optimize the experimental conditions (resolution versus angular interval). Typical exposure time was 10– to 30 seconds. The setup was calibrated with lanthanum hexaboride (LaB_6) and/or silicon powder.

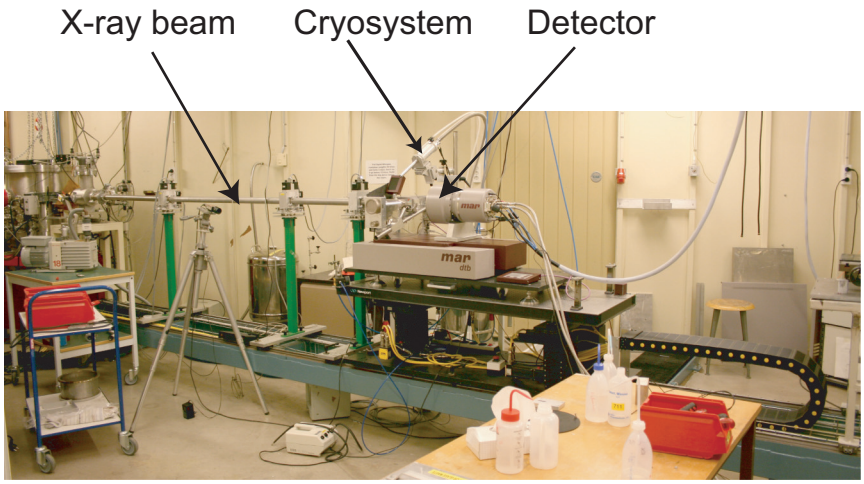

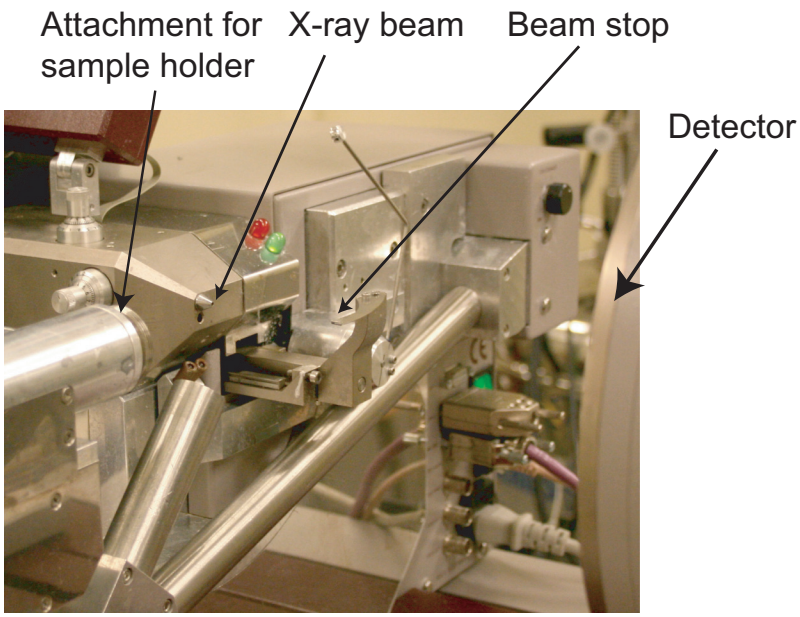

Figure 9. Experimental setup used for XRD and SAXS at beamline I711, MAX-lab, Lund University.

Small angle X-ray scattering (SAXS)

SAXS data was collected at the beamline I711 at MAX-lab, Lund, Sweden. The SAXS setup was almost identical to the XRD setup at the I711 beamline, the main difference being that a much larger sample - detector distance was used (1643 mm compared with approx. 250 mm). Silver behenate (AgBEA) was used to calibrate the wavelength, as silicon or LaB_6 do not have any reflections at low angles. Because of the longer sample-detector distance the X-ray beam travelled inside an evacuated tube to avoid air scattering. The low pressure during the evacuation of the air in the tube was sometimes problematic, as the wax sealing of the capillaries broke, causing the water to evaporate from the water rich clay samples.

X-ray absorption near edge structure (XANES) spectroscopy

X-ray absorption spectroscopy data were collected at the beamline I811 at MAX-lab, Lund, Sweden (**Carlson *et al.* 2006**). X-ray absorption spectroscopy is divided into different energy intervals in relation to the absorption edge. In XANES only the vicinity of the absorption edge is studied, whereas in EXAFS (extended X-ray absorption fine structure) a much wider energy interval is used in the measurement. In Fe K-edge XANES the energy of the K-shell electrons in Fe is measured, and it depends on the oxidation state of the iron. XANES has been used to characterize the oxidation state of iron in various geological, archaeological and biological samples using either the intensity and position of the pre-edge or the position of the main absorption edge (**Paris *et al.*, 1991; Galoisy *et al.*, 2001; Wilke *et al.*, 2001, 2005; Kwiatek *et al.*, 2001; O´Day *et al.*, 2004; Quartieri *et al.*, 2005**). Depending on the concentration of iron in the sample either fluorescence data or absorption data were used. During the measurement three ion chambers were used (**Figure 10**) to measure the X-ray intensity before and after the sample and also after an iron reference foil used for energy calibration. The bentonite was placed between XRF-tapes during the measurement. Three consecutive scans (~120 seconds each; 0.33 eV step size) were recorded over the range -150 to +500 eV (relative to the absorption edge) and merged and analysed as an average unless otherwise stated. The tapes and the rapid measurement minimized sample oxidation during the measurement and also allowed more samples to be analysed within a certain time. Additionally to the position of the K-edge absorption there are also other diagnostic features present, such as pre-edges and overall structure of the absorption curve that are related to other parameters such as coordination number and neighbouring atoms. The data was evaluated by

comparing the sample data with data from reference compounds with known oxidation state, and by linear combination a semi-quantitative determination of the Fe(II)/Fe-total ratio was performed. There are other techniques for measuring Fe(II)/Fe(III) such as Mössbauer spectroscopy that also give other complementary information (*e.g.* **Murad and Cashion, 2004**). Some advantages with XANES are the possibility of shorter measurement time and the ability to measure also other elements of interest such as Cu.

(a)

(b)

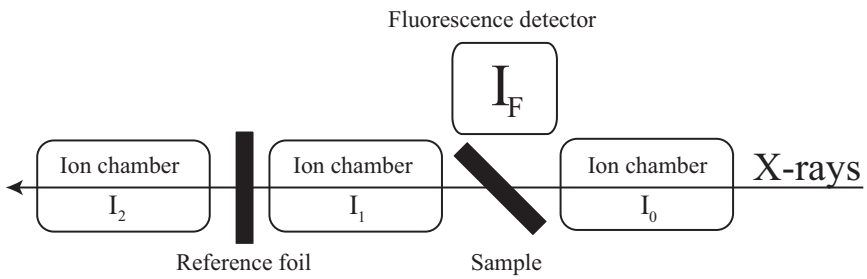

Figure 10 (a) Picture of the I811 experimental hutch used for XANES data collection at MAX-lab. (b) Explanatory sketch marking incoming X-rays from the right, ion chambers, the sample and the reference foil positions.

Chemical reduction of trivalent iron in montmorillonite

Poorly crystallized phases of *e.g.* iron, aluminum and silicon may be dissolved by reductive dissolution using sodium dithionite in a citrate-bicarbonate solution. Analysis of the solution gives quantitative information about the number of dissolved phases and, as the remaining sample has fewer phases, further analysis is less complex (**Mehra and Jackson, 1958**). The trivalent iron in the smectite is however also partly or fully reduced to divalent iron by the reaction. The solution should be removed from the clay afterwards as it contains dissolved iron and the sample should then carefully be dried in an anaerobic glovebox to avoid re-oxidation. By reacting well dispersed Wyoming Na-montmorillonite at 80 °C for four hours using a magnet stirrer and a constant purge with argon a montmorillonite highly dominated by Fe(II) was produced (**Figure 11; Svensson and Hansen, 2013b**).

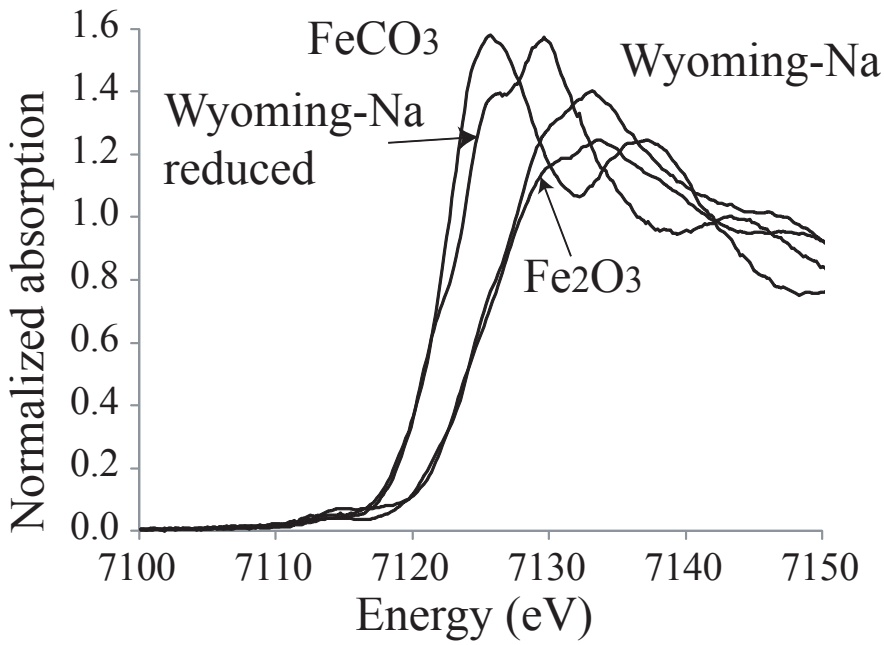

Figure 11. XANES spectra of natural and artificially reduced Wyoming montmorillonite compared with $Fe(II)CO_3$ and $Fe(III)_2O_3$ (**Svensson and Hansen, 2013b).**

Field experiments at Äspö Hard Rock Laboratory

Alternative Buffer Material experiment (ABM1 and ABM2)

The experiment was installed in 2006 and a total of three packages were installed (**Eng *et al.*, 2007**). The first one (ABM1) was excavated in 2009 (**Svensson *et al.*, 2011; Svensson and Hansen, 2013b**) and the second (ABM2) in 2013 (**Svensson, 2013**). The experimental layout was similar to the Swedish KBS-3 concept except for the much smaller scale and the use of iron instead of copper as a heater material (**Figure 12**). The temperature was also higher, 130 °C instead of below 100 °C. The experiment included 11 different compacted clays of various qualities and was wetted by both natural water from fractures in the rock and by an installed water saturation system using natural formation water.

Temperature Buffer Test experiment (TBT)

The experiment was installed in 2003 (**Sandén *et al.*, 2007**) and was excavated in 2010 (**Åkesson *et al.* 2012**). The design and scale of the TBT experiment were very similar to a KBS-3 type installation with the exception of the heater material (carbon steel) and temperature (150 °C). The water saturation pressure was controlled by pipes in a sand filled slot between the bentonite buffer and the rock (**Figure 12**).

The Prototype Repository

The Prototype experiment is a full scale experiment and was installed with six copper canisters distributed in an inner and an outer section (4+2 canisters). Between the inner and the outer section a concrete plug was installed and the tunnel was backfilled with a mixture of bentonite and crushed rock (30 wt% bentonite). The experiment was installed in 2001-2003 (**Svemar *et al.*, 2013**), and the outer section (canister 5 and 6) was excavated in 2011 (April to December). The studies done within the work of this thesis were performed on bentonite from deposition hole 6 (dh6) and reported in **Olsson *et al.* 2013**.

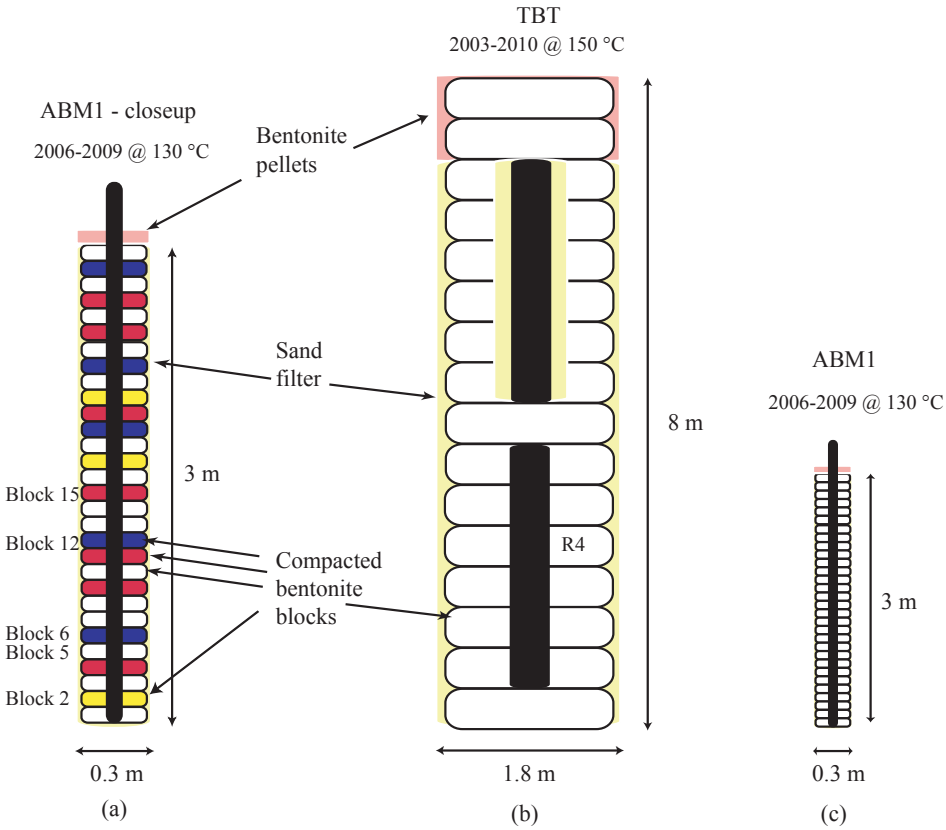

Figure 12. Illustration of the ABM and TBT experiments. The location of the various samples used in this study are marked. (a) ABM1 - close up with details (several different bentonites) (b) TBT (only MX-80 bentonite) and (c) ABM1 in true scale compared with TBT.

The bentonite barrier - Swelling properties

A sample of wet smectite clay exposed to the atmosphere in the lab will dry, but not become totally anhydrous. However, a smectite dried at 300 °C for two hours is considered to be totally anhydrous (**Brindley and Brown, 1980**). In this state there is no interlayer water and the interlayer distance is approximately 9.6 Å. If equilibrated to ambient atmosphere (30 to 50% relative humidity, RH) the interlayer distance will be approximately 12.5 Å (one-water-layer hydrate; W1) with sodium as interlayer cation, and approximately 15.2 Å in the case of calcium (two-water-layer hydrate; W2; **Brindley and Brown, 1980**). The larger interlayer distance is owed to water hydrating the interlayer cations and the silicate surfaces (**Figure 13**).

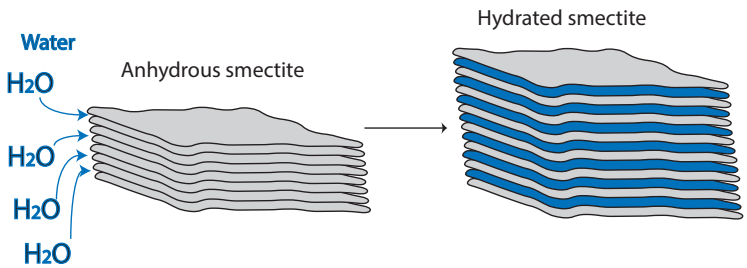

Figure 13. A highly schematic illustration of water intercalation and crystalline swelling of smectite.

The expansion from *e.g.* 9.6 to 12.5, 15.5 or 19.2 Å is called crystalline swelling, and the magnitude of this swelling is a function of several factors. The smectite basal distance is seen to change in discrete steps of approximately 2.9 Å, which corresponds to the approximate diameter of a water molecule. However, the observed basal distance may change in a continuous fashion in a W2-W3 interstratified system, if the ratio of W2 and W3 is gradually changed. If smectite is placed in deionized water the calcium form will swell to approximately 19 Å and the sodium form will swell well beyond that (**Figure 14**). The distance between the layers in the sodium smectite is then less well defined as the tactoids delaminate (separate) and this state is called osmotic swelling (we denote this as WX when the exact hydration stage is unspecified). This difference in swelling behavior can be

seen by using X-ray diffraction as well as macroscopically in swelling experiments (**Figure 14**).

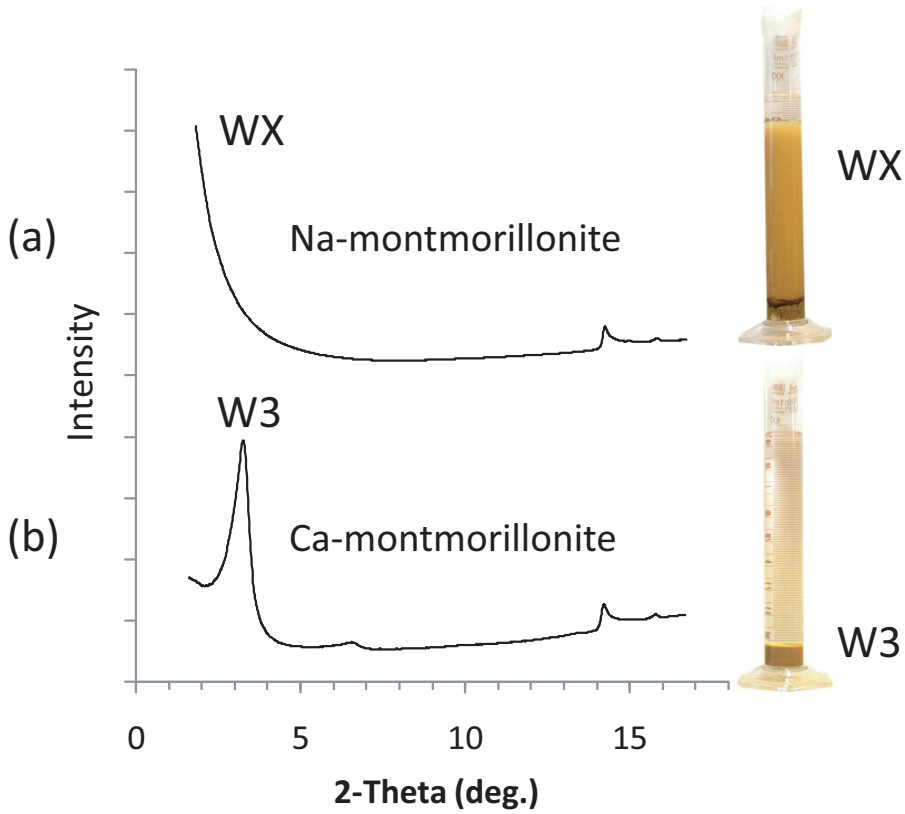

Figure 14. X-ray diffractograms of wet clays (left) and swelling tests (right). (a) Wyoming Na-montmorillonite in water showing osmotic swelling (WX). In the glass cylinder is a natural sodium-dominated bentonite (Asha 505) from the Kutch area, India. (b) Wyoming Ca-montmorillonite in water. In the glass cylinder is a natural calcium-dominated bentonite from Rokle, Czech Republic.

Heterogeneity may exist in both wet systems as well as in compacted bentonite and different micro-structural models have been proposed (**Pusch and Yong, 2003**) and the ageing effects of this microstructure have also been discussed (**Delage *et al.*, 2006**). **Holmboe *et al.* (2012)** investigated the heterogeneity with respect to a double porosity model, and evaluated the relation between interlayer porosity and inter-particle porosity in compacted and water saturated bentonite samples (densities of 1.4-1.8 g/cm^3), and found that the interlayer porosity totally dominated, and the interparticle porosity (excess porosity) was estimated at ≤ 3%.

Keller *et al.* (**2014**) investigated the open porosity in compacted bentonite in the ABM1 experiment (**Svensson *et al.* 2011**) with focused ion beam nanotomography and found the unsaturated starting material to have a porosity of 4.3-4.6 vol.%, which was reduced to < 1 vol.% after the experiment, due to the swelling of the clay. Hence, there is no strong evidence of any significant interparticle porosity in a confined water saturated bentonite at high density. To summarize: when equilibrated to ambient atmosphere calcium smectite will swell more than sodium smectite; on the other hand, in contact with liquid water the opposite will occur. This indicates that there are several factors controlling the swelling of the smectite, and depending on the situation the dominant force may change. This has some implications for the bentonite buffer in a KBS-3 repository as the swelling pressure of Ca and Na bentonite varies, especially in the low-density region (**Karnland *et al.*, 2006**).

Crystalline swelling of smectites with divalent interlayer cations

The following section focus on the swelling of smectites in liquid water and focus on the case with divalent interlayer cations. However, Na-montmorillonite in 3 M NaCl is also included for comparison as it behaved similarly. The crystalline swelling of smectites is balanced between the energy needed to expand the structure in relation to the energy released from the hydration process (**Suzuki *et al.* 1987; Slade *et al.* 1991**). At least the following parameters contributes to the crystalline swelling in the case with free access to liquid water: (1) the electrostatic interaction between the positive interlayer cations and the negative phyllosilicate layer, (2) osmotic pressure and energy release by hydration of the smectite phyllosilicate surfaces and the interlayer ions and solutes, (3) the van der Waals attraction between the phyllosilicate layers and (4) the attractive and anisotropic ion-ion correlation forces between the interlayer cations (**Kjellander *et al.* 1988**). In the range of crystalline swelling the van der Waals attraction is regarded to be very small compared with the electrostatic interaction (**Suzuki *et al.* 1987**).

Temperature

Most freezing studies of the montmorillonite-water system have focused on the freezing process where ice forms and the montmorillonite dehydrates (*e.g.* **Norrish and Rausell-Colom, 1962; Ahlrichs and White, 1962**). Instead we now focus on what happens to the montmorillonite hydration before the ice forms. In **Svensson and Hansen (2010b)** and in **Svensson and Hansen (2014),** an increase in the basal spacing of Wyoming Ca-montmorillonite was seen during cooling from 19 Å to a combination of 19 Å and 21 Å (**Figure 15**; the ice formation later dehydrated the montmorillonite to a 16 Å W2-hydrate). A similar expansion upon cooling was also seen with salt solutions (**Svensson and Hansen, 2013a**) both for Ca-montmorillonite (**Figure 16**) and for Na-montmorillonite (**Figure 17**).

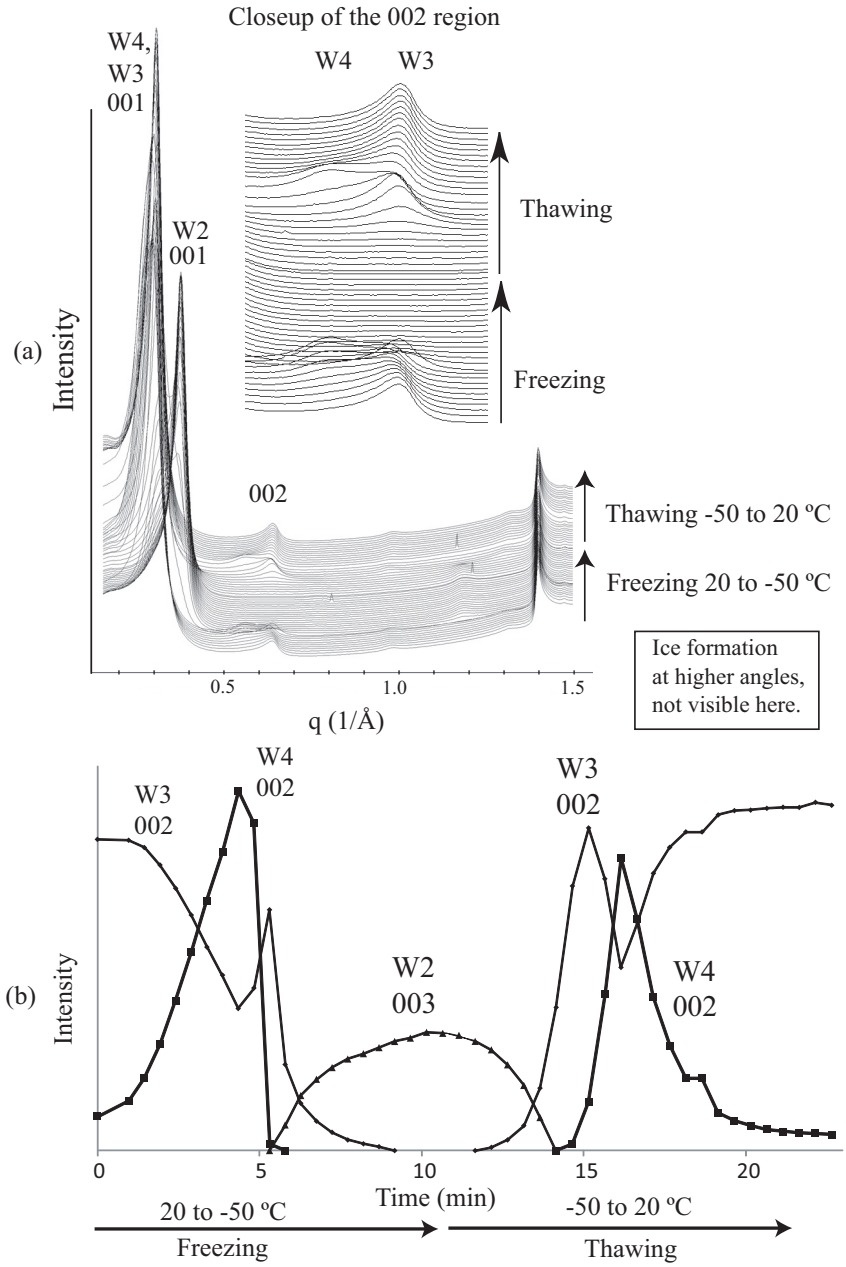

Figure 15. Freezing and thawing of Wyoming Ca-montmorillonite (from MX-80; 30 wt% in water). (a) X-ray diffractograms of freezing and thawing, with a close-up of the 002 reflection region. Ice reflections are at higher angles and are not seen in this experiment. (b) Integrated intensity of W4 and W3 002 reflections as a function of time (**Svensson and Hansen, 2014**).

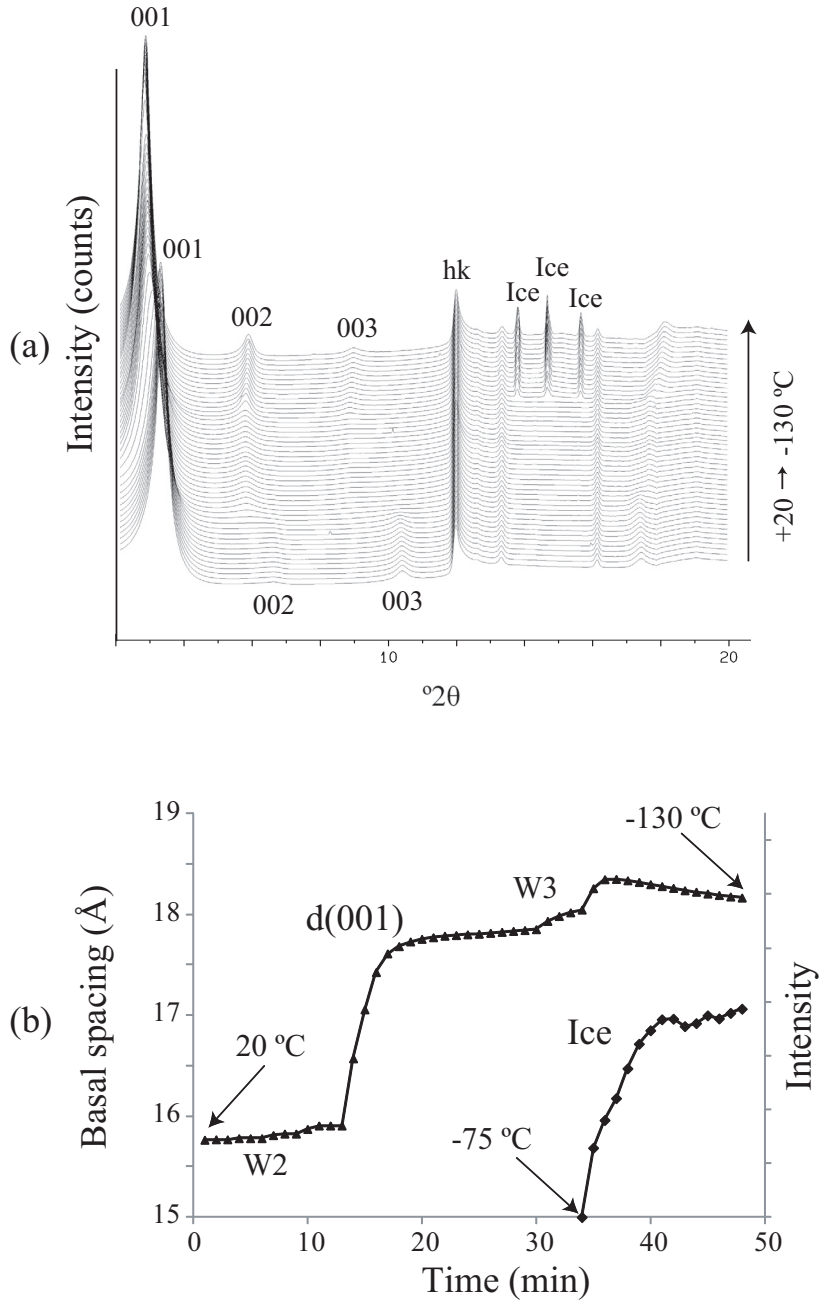

Figure 16. Freezing of Ca-montmorillonite (30 wt%) in 3M $CaCl_2$ from +20 to -130 ºC resolved in time. (a) Consecutively recorded diffractograms and (b) basal spacing and ice intensity as a function of time (temperature). λ = 0.955 Å (**Svensson and Hansen, 2013a**).

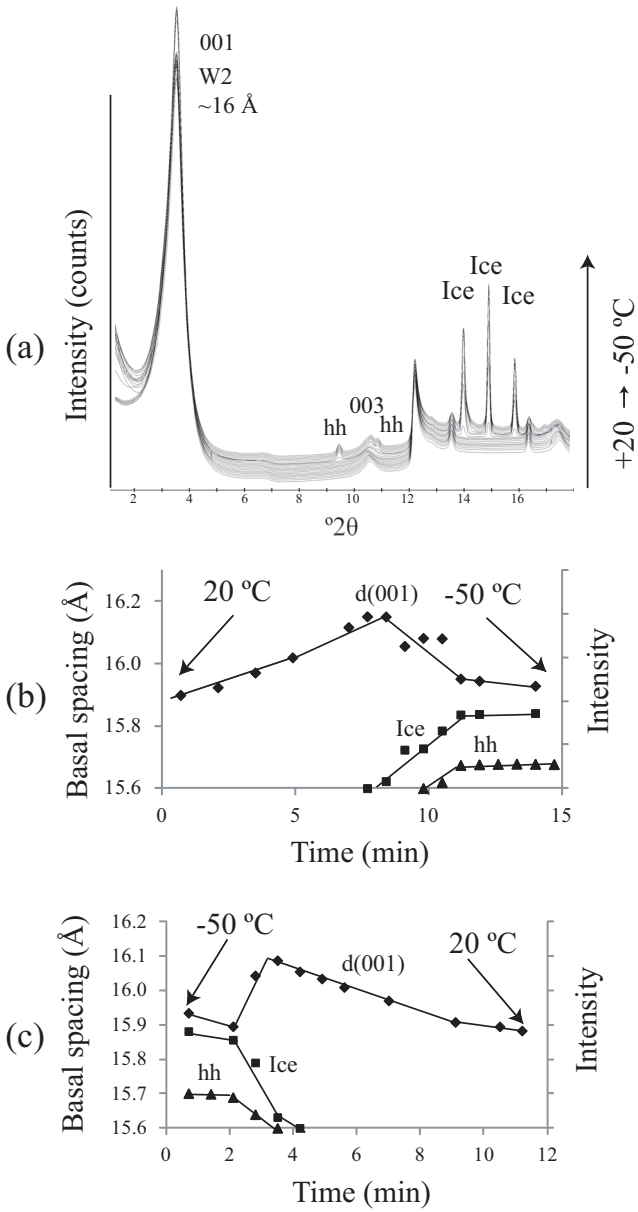

Figure 17. (a,b) Freezing of Na-montmorillonite (30 wt%) in 3M NaCl from +20 to -50 ºC resolved in time (c) thawing from -50 to 20 ºC (λ = 0.955 Å). Hydrohalite is abbreviated as hh (**Svensson and Hansen, 2013a**).

Wyoming Ca-montmorillonite in 3M $CaCl_2$ was most extreme and started at 15.5 Å (W2) at 20 °C and expanded during the cooling to 18.2 Å (W3) before the ice formation started (at approximately -70 °C; **Figure 16**). The Wyoming Na-montmorillonite in 3M NaCl also expanded; however, the expansion was much smaller, from 15.9 Å at 20 °C to 16.1 Å before the ice formation (**Figure 17**). The increase in swelling at decreased temperature proposed that the opposite would occur at increased temperature, and as predicted, decreased swelling was observed at increased temperature in Wyoming Ca-montmorillonite by repeated cycling of the temperature up and down (20 to 60 or 90 °C and back; **Figure 18**). These observations are analogous to what has been observed in swelling pressure measurements during decreasing temperature (**Birgersson *et al.* 2008**), were the swelling pressure somewhat increased with lower temperatures and, as the ice formed in the external reference water, the swelling pressure rapidly decreased. On the other hand, **Zhang *et al.* (1993)** concluded that the basal spacing was "essentially independent" of the temperature when saturating through the gas phase (no direct contact with liquid water); however, the maximum water uptake by the montmorillonite decreased with increased temperature.

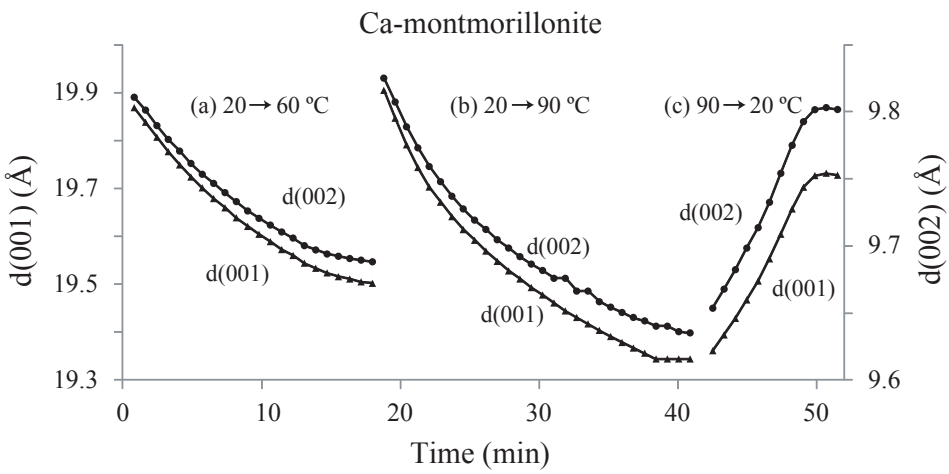

Figure 18. Ca-montmorillonite (30 wt% in water) basal spacing as a function of temperature given as d(001) (dots) and d(002) (triangles). Three consecutive series: (a) 20 → 60 °C, (b) 20 → 90 °C and (c) 90 → 20 °C (**Svensson and Hansen, 2013a**).

Hatharasinghe et al. (2000) observed the expansion during cooling (+5 to -5 °C) of a mixture of butylammonium vermiculite, butylammonium chloride and water. At 1 °C the intensity of the 001 reflection increased and simultaneously shifted towards lower angles (indicating an expansion of the smectite) and later at 0 °C the intensity again decreased. This observation was, however, not further discussed. In the results of **Anderson and Hoekstra (1965)** a small (0.4 to 1.3 Å) but systematic increase in basal distance was seen in the 001 spacing of Ca-Wyoming montmorillonite by stepwise lowering of the temperature (steps of 1 °C, from +4 to -20 °C). This small change was, however ignored by the authors and the diffractograms had a far too low signal-to-noise ratio to identify any overlapping 001 reflections or even to see the 002 reflections. Hence, it seems to be a general trend that hydration of montmorillonite and its interlayer cation increases at lower temperatures and decrease at higher, even with free access to water. This is true not only for montmorillonite but also for pure salt-water systems. **Zavitsas (2005)** studied the $CaCl_2$ –H_2O system and observed that the hydration of Ca^{2+} increased at lower temperatures. At least three processes are assumed to be involved in the temperature dependence on the crystalline swelling in solution before the formation of ice: (1) the temperature impact on the Gibbs free energy of the hydration reaction, (2) the temperature impact on the dielectricity constant (ε), as it affects the Coulombic interaction between the negative montmorillonite sheets and the positive interlayer cations, and (3) the thermal contraction owed to the decrease in thermal vibrations at lower temperatures. The Gibbs free energy equation describes the conditions for a spontaneous chemical reaction to occur ($\Delta G<0$), and is a balance between the enthalpy and the entropy of the reaction (**Atkins, 1998**):

$$\Delta G = \Delta H - T\Delta S \qquad (3)$$

At reduced temperatures the entropic term ($T\Delta S$) is also reduced and the enthalpy (ΔH) of the reaction becomes more dominant, and the somewhat incompletely hydrated interlayer cations may hence hydrate further (exothermic process with $\Delta H < 0$).

As the montmorillonite layers and the interlayer cations are separated, work is needed to counteract the attractive force of interaction (F) between the positive charge of the interlayer cations (Q_1) and the negative charge of the montmorillonite sheets (Q_2) and is described by Coulombs law (**Atkins, 1998**):

$$F = Q_1Q_2 / (4\pi \varepsilon r^2) \quad (4)$$

As the interlayer distance (r) increases, the electrical interaction decreases, and as the temperature decreases (+20 ºC to 0 ºC) the dielectric constant ε increases from 80.2 to 87.9 (**Owen *et al.*, 1961**). Such increase decreases the electrostatic interaction; hence, less energy is assumed to be needed to expand the montmorillonite structure. Additionally, a decrease in temperature will contract the material by thermal contraction. The thermal contraction can be estimated with the thermal expansion coefficient (α ; **Benson, 1995**):

$$\alpha = \Delta L / (L_0 \Delta T) \quad (5)$$

where ΔL is the change in length compared with the original length (L_0) as the temperature changes over a specific interval of ΔT. Expansion coefficients for muscovite and pyrophyllite are in the range of 0.18×10^{-4} and 0.15×10^{-4} K^{-1}, respectively (**McKinstry, 1965**). The impact on water saturated montmorillonite (e.g. W3) can be estimated if one assume an intermediate (muscovite-pyrophyllite) expansion coefficient for the montmorillonite layer and assuming that interlayer water behaves like normal water. The montmorillonite layer is expected to contract at lower temperatures, whereas the interlayer water is expected to have a more complex behavior as the water density is at its maximum at 4 °C (Table 1).

Table 1. Estimated thermal impact on the basal spacing of montmorillonite (W3). Specific volume of water from Kell (1967). Assuming 10 Å of water at 20ºC.

T / ºC	Montmorillonite layer /Å	Interlayer water /Å	Total /Å
20	9.6000	10.0000	19.6000
4	9.5974	9.9823	19.5797
0	9.5967	9.9837	19.5804
-20	9.5934	10.0477	19.6411

The layer charge (total and distribution)

A four-water-layer hydrate (W4) at ~21 Å formed during various conditions in the Wyoming montmorillonite, both when prepared from the commercial MX-80 bentonite as well as when prepared from the SWy-2 CMS source clay. The W4 hydrate was, however, not formed by Milos or Kutch smectites, indicating that fundamental differences between the smectites were present. The Milos and Kutch smectites were also affected by the decreased temperature, however to a much smaller extent. Among the included smectites, lower layer charge (**Figure 19a**) and/or higher amount of the charge present in the octahedral sheet (**Figure 19b**) gave a higher basal spacing than smectites with higher layer charge and/or lower amount of the charge present in the octahedral sheet, based on layer charge calculations from chemical composition of the clay fractions (**Karnland *et al.*, 2006**). The trend that smectite with a lower charge seems to swell more is also seen in several other datasets such as **Brindley and Brown (1980)**, **Slade *et al.* (1991)** and **Suquet *et al.* (1975)**. **Laird (2006)** concludes that beyond a certain threshold value, the attractive forces increase more than the repulsive forces as the smectite layer charge increases.

Most likely, only smectite with a total layer charge below a certain threshold value, and/or high fraction of the charge originating from substitutions in the octahedral sheet, can expand to W4 (*e.g.* with Ca and low temperature). This indicates that the layer charge in Wyoming montmorillonite could be heterogeneously distributed, with some of the montmorillonite having a lower charge forming W4 and some a higher charge forming W3. Such heterogeneously distributed layer charges have been described by **Lagaly (1979)** and **Christidis and Eberl (2003)**. Various possibilities exist for a heterogeneous distribution, such as interstratification (ordered or disordered) of layers of varying total charge, different charges on the up and down sides of individual layers, and lateral variations within each layer. Hence, a lower layer charge seems to decrease the work needed to expand the structure and seems to result in a larger crystalline swelling under the circumstances investigated here. The < 0.06 µm size fraction in Wyoming bentonite seems to have lower layer charge than that seen in the 0.06-0.6 µm size fraction (**Lagaly, 1994**). Possibly this low charge fraction is the reason for the W4 observed in Ca-Wyoming montmorillonite (**Figure 15**). Lagaly (1994) reports a charge of -0.56 for Wyoming montmorillonite (based on the alkylammonium ion method), and **Christidis and Eberl (2003)** report -0.72 (structural formula method) and -0.79 (K-saturation and EG swelling method).

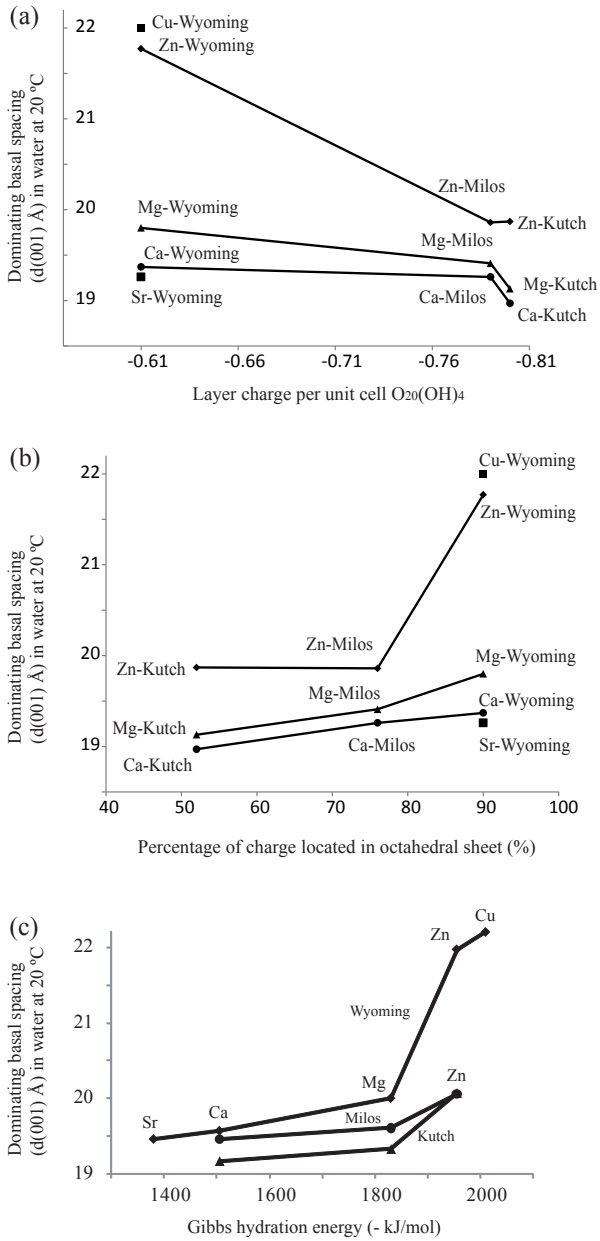

Figure 19. Dominating basal spacing of smectites in liquid water (30 wt% smectite) with divalent interlayer cations as a function of (a) total layer charge, (b) layer charge distribution and (c) Gibbs hydration energy of the interlayer cation (**Svensson and Hansen, 2014**).

Divalent interlayer cations

In the Ca- and Sr- Wyoming montmorillonites the W4 phase appeared at a low temperature prior to freezing; however, in the Mg-, Cu- and Zn- Wyoming montmorillonites W4 was already partly present at room temperature (Mg: W3>W4; Cu, Zn: W4>W3). Hence the type of divalent cation clearly affected the ability to form W4 and also the maximum swelling in water of the smectites at 20 ºC. The general trend in basal spacings at 20 °C was: Wyoming: Cu > Zn > Mg > Ca > Sr, Milos: Zn > Mg > Ca, and Kutch: Zn > Mg > Ca. The dominating basal spacing at 20 ºC for a specific smectite was highly related to the Gibbs hydration energy of the interlayer cation (**Figure 19c**; Gibbs hydration energy values from **Marcus, 1994**). In the interlayer the cations are partially hydrated (in equilibrium with the attractive forces), and the greater the hydration energy of the cation, the more extensive hydration may take place under otherwise fixed conditions.

Summary

The crystalline swelling of the investigated smectites with free access to liquid water was found to different extent to:

-Increase at lower temperatures until freezing occurred. The temperature effect was interpreted as a combination effect of the impact on the equilibrium between entropy and enthalpy of the hydration reaction and/or the temperature dependence of the dielectric constant.

-Decrease with increased smectite layer charge and/or amount of charge originating from the tetrahedral layer. This was interpreted as increased layer charge increased the attraction between the layers and counteracted the swelling.

-Increase with increasing Gibbs hydration energy of the interlayer cation. The more energy that is released by the hydration the further the smectite can swell.

Osmotic swelling of smectites in water

There are mainly two regions of swelling for smectites, crystalline swelling with one to four layers of water and osmotic swelling caused by delamination of the tactoids into smaller tactoids or even into single platelets. The driving force in osmotic swelling is the gain in entropy by the process, and the forces involved are not equal to the ones involved in crystalline swelling. It is well known that Na-montmorillonite swells osmotically when placed in water (**Norrish, 1954; Fukushima, 1984**). The resulting basal spacing is restricted mainly by the clay/water ratio (**Figure 20**) and can at higher spacings (>40 Å) be calculated as the sum of the volume of the dry clay and the volume of the water (**Svensson and Hansen 2013a**). Both Li-saponite and Li-beidellites have been found to swell osmotically; however, there are examples of Na-saponite and Na-beidellites that do not (**Suquet *et al.* 1975**). Hence, minor differences in the interlayer cation properties, the total layer charge and/or charge position seem to be important. **Hansen *et al.* (2012)** have studied Na-fluorohectorite with large lateral dimensions (~µm) and a high intrinsic layer charge and found that the swelling in this case is restricted to the crystalline swelling region with a maximum basal spacing of 15.1 Å (W2) in stacks of about 100 platelets. However, by increasing the temperature to 78 °C they found the Na-fluorohectorite delaminated and swelled to interparticle distances of ~180 Å. By means of theoretical model calculations the temperature-driven expansion can be explained by the entropy gain of the free counter ions with temperature.

Montmorillonite with divalent interlayer cations is known from XRD data to have a swelling restricted to the region of crystalline swelling (**Norrish, 1954**). SAXS data on smectites with divalent interlayer cations confirm crystalline swelling with free access to water with 001 reflections at round 19 to 20 Å (**Figure 21**); however, an additional osmotic component could possibly be present in the low angle region and revealed as an intensity increase, similarly to what is observed in the 10 wt% Na-montmorillonite case (**Figure 20**). In other words, it is easy to identify osmotic swelling if no basal reflection is present at ~20Å; however, a combination of osmotic swelling and crystalline swelling would be more difficult to identify, *e.g.* if the tactoids were only partly delaminated or decreased in thickness, as the observed scattering is a function of both how the measurement is performed (method) and the material properties.

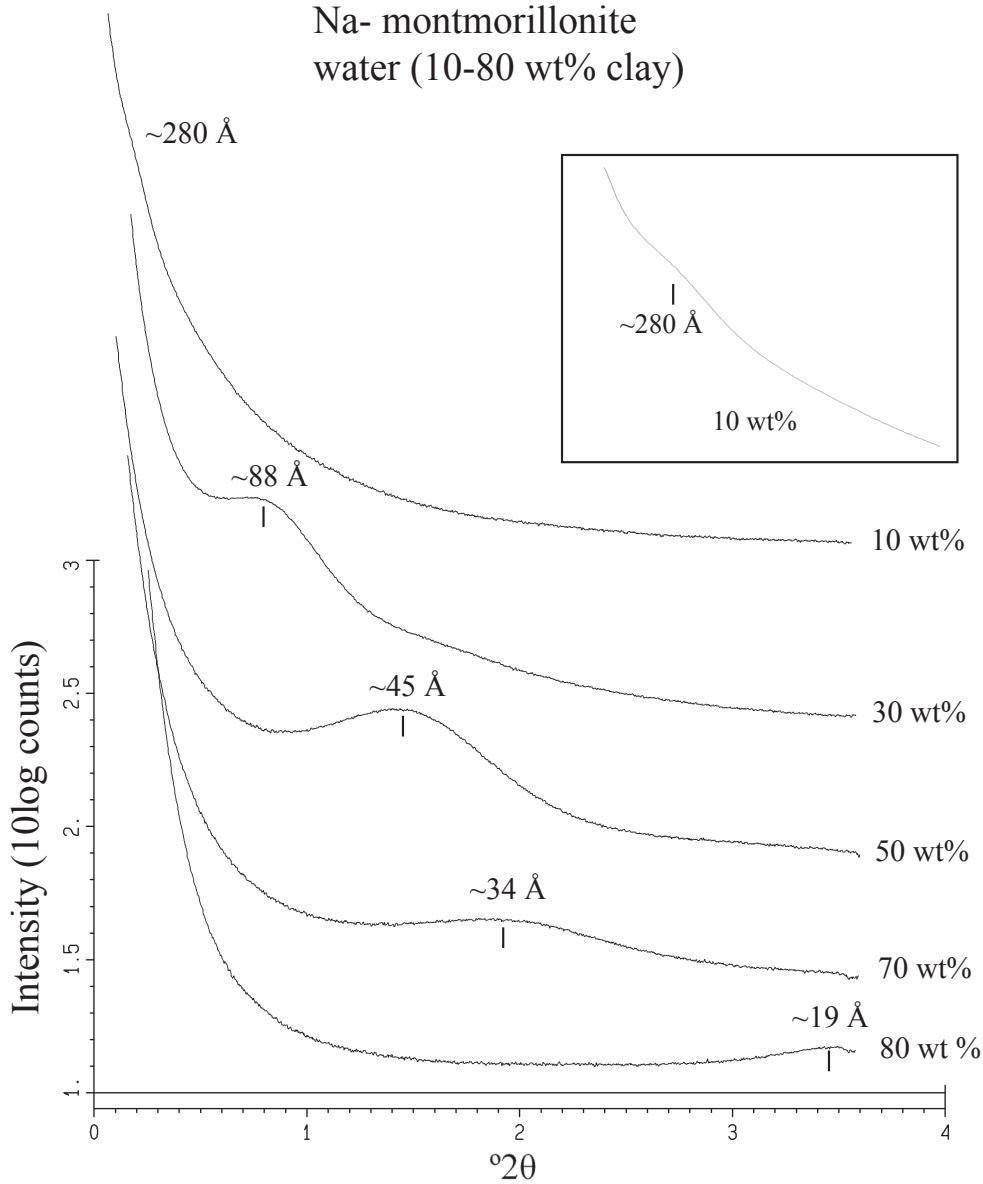

Figure 20. Small angle scattering of Wyoming Na-montmorillonite, showing the relation between basal spacing and water content (**Svensson and Hansen, 2013a**). λ = 1.09994 Å.

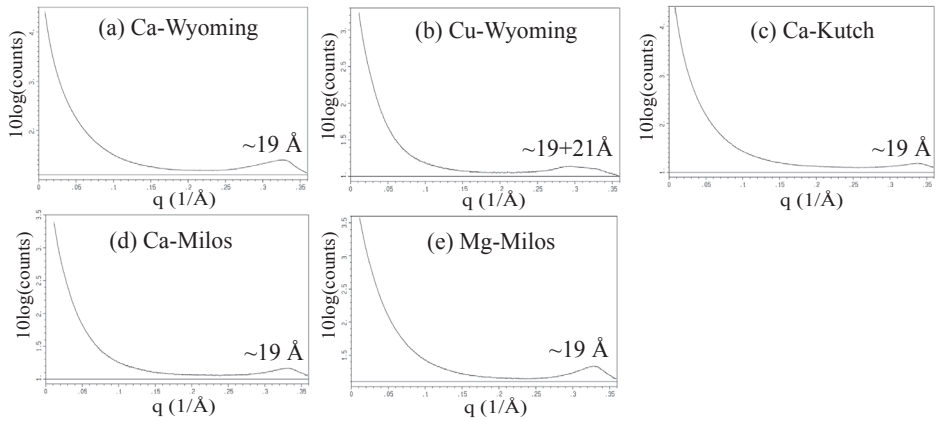

Figure 21. SAXS data of a selection of smectites with divalent interlayer cations (30 wt% in water) showing a maximum crystalline swelling of approximately 19 to 21 Å (**Svensson and Hansen, 2014**). λ = 1.09994 Å.

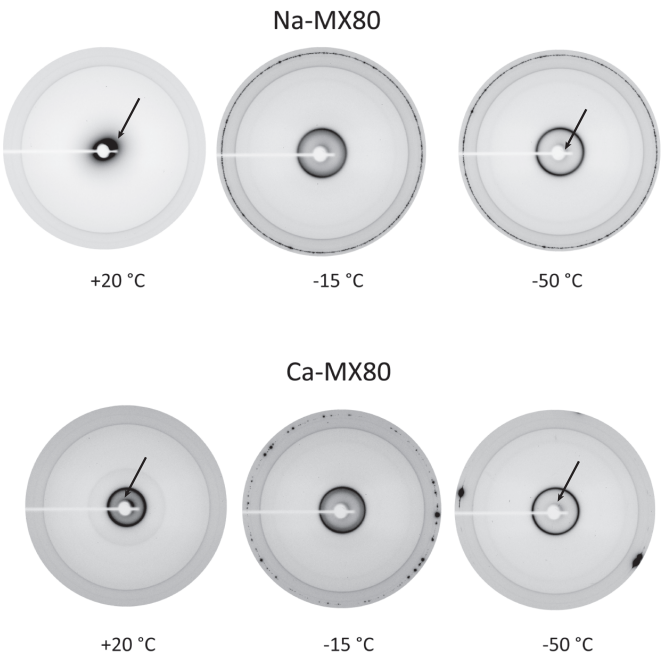

Figure 22. Two dimensional diffractograms of clay pastes with pure water at +20, -15 and -50 °C. The peripheral ring/spots at low temperatures comes from ice. The low angle scattering discussed in the text is marked by an arrow (**Svensson and Hansen, 2010b**).

There are however measurements which indicate that there really is a contribution of osmotic swelling in divalent systems. A theoretical average layer distance can be calculated in a system with known volume, dry density and grain density of the smectite. A swelling pressure of 13 kPa was achieved by saturating a compacted Milos Ca-smectite with a dry density of 522 kg /m^3 (**Karnland *et al.* 2006**). The presence of swelling pressure indicates that the smectite occupies the entire volume and has a tendency to hydrate even further. In such a system the porosity can be calculated as (1 – 522/2750) x 100% = 81%, if the grain density is assumed to be 2750 kg /m^3. This indicates that the hydrated smectite has 2750/522 = 5.3 x larger volume than anhydrous smectite. The basal spacing of an anhydrous smectite is about 9.6 Å. If the system is totally homogeneous the average calculated interlayer distance is 9.6 x 5.3 = 50.9 Å. However, as mentioned earlier, the Ca-smectite only swells to 19 Å according to XRD and SAXS data.

Segad *et al.* (2010) performed water uptake measurements on Ca Wyoming montmorillonite from water placed inside dialysis bags, and on the basis of maximum water uptake they estimated the average swelling to be ~100 Å. However, in the SAXS data no 100 Å reflection could be identified. From the peak width in the X-ray scattering curves of the ~20 Å 001 reflection they estimated the number of platelets per tactoid to between 10 and 20 in the Ca-montmorillonite. From this estimation and the data from the water uptake experiments they calculated an inter-tactoidal distance of 500 to 1000 Å, which was far greater than could be seen in the SAXS data.

In **Svensson and Hansen (2010b)** changes in the low angle scattering were found in Wyoming Ca-montmorillonite when the water was frozen into ice by decreasing the temperature from +20 to -50 °C (**Figure 22**). This could be a sign of inter-tactoidal swelling and was rather similar to what was seen in the Na-montmorillonite case; however, in Ca-montmorillonite an additional 001 reflection at ~20 Å from the crystalline swelling was also observed.

The data discussed indicates that the system may not be homogeneous and both crystalline and osmotic swelling seems to occur side by side. **Jönsson *et al.* (2009)** also concludes similarly on this topic, that the swelling most likely is divided in two components, one intra-lamellar and one extra-lamellar, and that the extra-lamellar swelling is currently poorly understood.

Summary

Osmotic swelling occur in montmorillonite in liquid water with monovalent interlayer cations at low to intermediate salinity. There are indications that osmotic swelling partly occur also in divalent systems in parallel with crystalline swelling, however no direct evidence based on X-ray scattering have been observed. The issue is interesting as the osmotic swelling is important at low buffer densities and is part of the mechanism behind what is called chemical erosion, were montmorillonite form colloid particles that in special cases may leave the deposition hole lowering the remaining density (**Jansson 2009**).

Surprising effects from salt on the freezing of montmorillonite

Several studies on the freezing of montmorillonite have been performed (*e.g.* **Norrish and Rausell-Colom, 1962; Ahlrichs and White, 1962; Birgersson *et al.* 2008**). In **Svensson and Hansen (2010b)** the dynamic freezing and thawing process was studied as a function of time (**Figure 23**), with the main focus on dehydration and rehydration coupled with contraction and expansion of the montmorillonite. At room temperature and when mixed with water (30 wt% clay in water) Na-montmorillonite was present as a free swelling hydrate (WX) and Ca-montmorillonite was present as a W3 hydrate at 19 Å. After the ice formation the montmorillonites (Na;Ca) dehydrated to W2+W3 (-15 °C) and to W2 at -50 and -100 °C (16 Å). This was very similar to what has been observed in the previous studies.

Natural groundwaters are however not deionised and contains more or less dissolved salts, and no previous study has been found on the influence of salt on the freezing of montmorillonite. In **Svensson and Hansen (2013a)** the basal spacings of montmorillonite in salt solutions at 20 °C were very similar to what has been previously reported (**Norrish, 1954**; **Amorim *et al.* 2007**). At 20 °C the Na-montmorillonite appeared as an osmotic WX phase (0 M) or had a basal spacing of ~19 Å (1 M NaCl; **Figure 24a**). In the case of Ca-montmorillonite the basal spacings were 19.4 Å (0 M) and 18.8 Å (1 M $CaCl_2$; **Figure 24c**). Hence, the introduction of salt decreased the basal spacing.

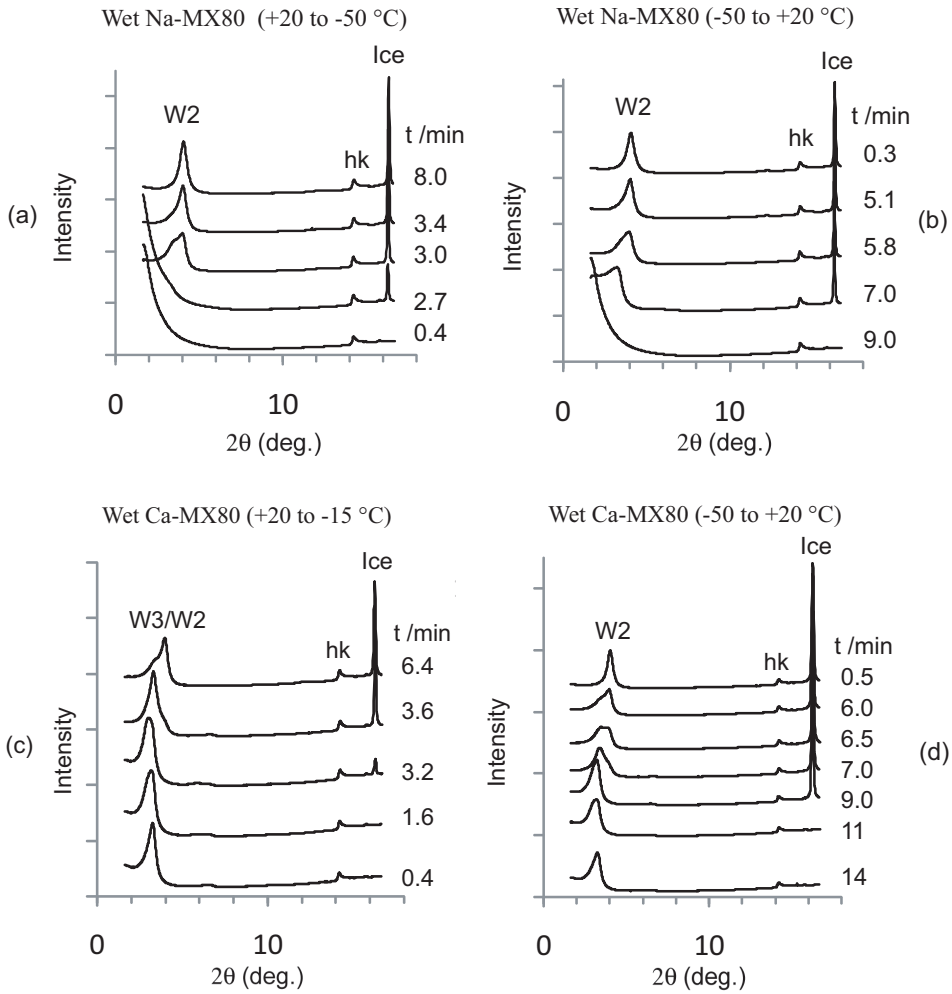

Figure 23. Time resolved freezing and thawing of Na- and Ca- montmorillonite (30 wt% clay in water; λ = 1.09994 Å; **Svensson and Hansen, 2010b).**

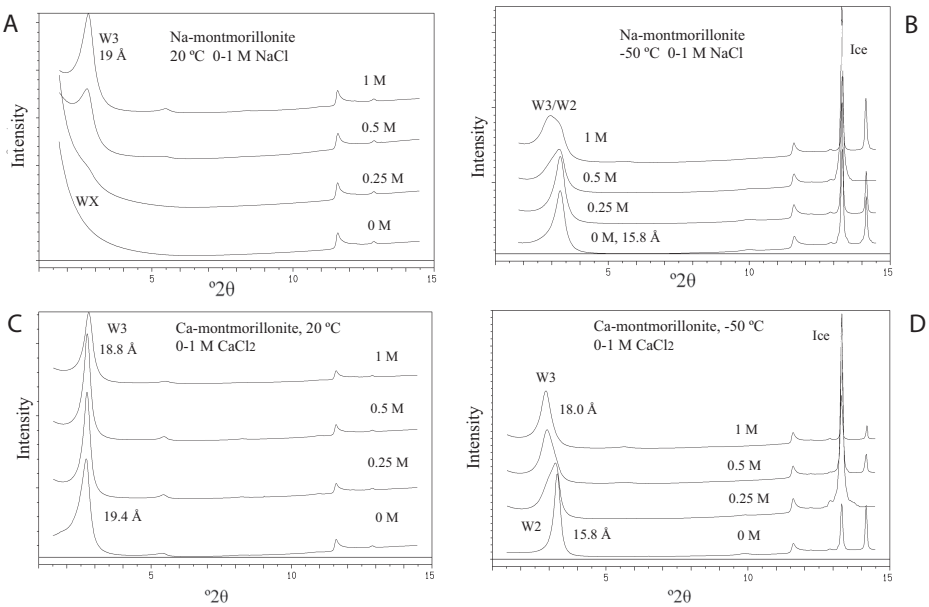

Figure 24. Powder XRD data of Na- and Ca-montmorillonite pastes (30 wt% solids) with 0 - 1 M electrolyte solution at +20 and -50 °C (λ = 0.9084 Å; **Svensson and Hansen, 2013a**).

In deionized water both Ca- and Na- montmorillonite after cooling to -50 °C dehydrated to W2 at ~16Å. However, with a salt solution the Ca-montmorillonite dehydrated only to ~18 Å upon freezing (**Figure 24d**) and the Na-montmorillonite to 16 Å or to 16 + 18 Å, depending on the initial salt concentration (**Figure 24b**). Hence, at room temperature the basal spacing was lowered by an increase in salt concentration, but at -50 °C the basal spacing was higher when salt was added, at least in the Ca- case. In the case of Na-montmorillonite in NaCl the basal spacing after freezing was higher at 1 M than at lower or higher concentrations (**Figure 25a**). The Ca-montmorillonite and $CaCl_2$ behaved somewhat similarly but maximum swelling occurred at -50 °C between 0.5 and 2 M (W3; ~18 Å; **Figure 25b**). At higher concentrations the basal spacing decreased somewhat but was still higher than what was found at 0 M and -50 °C.

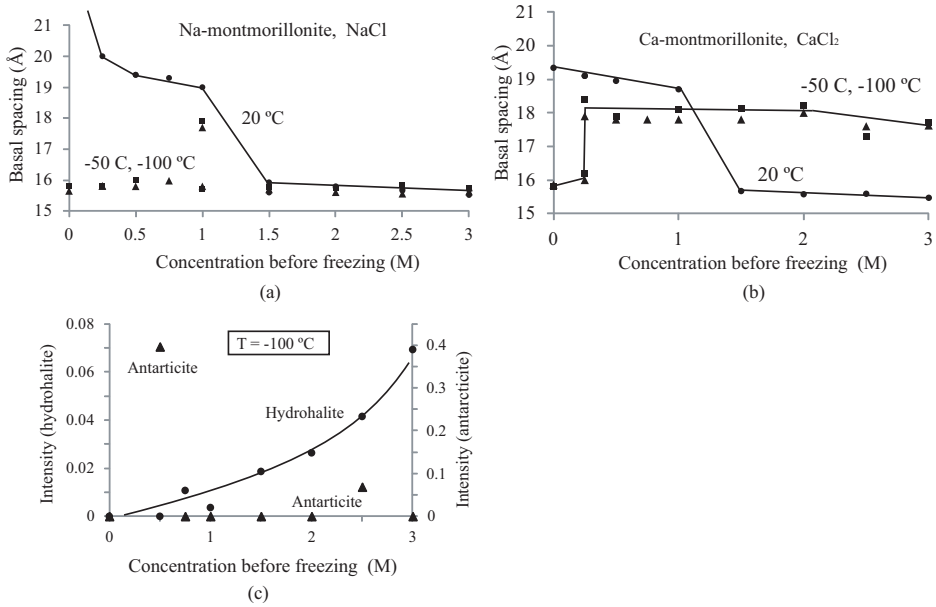

Figure 25. Basal spacing of montmorillonite as a function of starting electrolyte concentration at +20 ºC (dots), -50 ºC (squares) and -100 ºC (triangles) (a) Na-montmorillonite - NaCl, (b) Ca-montmorillonite - $CaCl_2$, (c) Hydrohalite and antarcticite formation at -100 ºC as a function of initial salt concentration (**Svensson and Hansen, 2013a**).

A maximum indicates that a small amount of salt increases the hydration at freezing temperatures (*e.g.* by introducing additional ions in the interlayer), whereas very high external concentrations decrease the swelling (*e.g.* by shifting the osmotic balance between the interlayer and the external solution or by affecting the dielectric constant). Hence, the salt either (1) changed the properties of the montmorillonite to hold water at low temperature, or (2) the salt changed the properties of ice at low temperatures. As long as the ice is pure the partial pressure of water vapor over the ice is unaffected by the external dissolved salt (**Schnewberger *et al.* 1978; Morillon *et al.* 1999**). No significant changes in the ice diffraction pattern in the data sets could be observed. This suggested that the properties of the ice were unchanged, but the properties of the Ca-montmorillonite changed after the salt addition.

The introduction of salt (cation and anion) into the montmorillonite interlayer owed to the Gibbs-Donnan effect has recently been discussed rather extensively (**Karnland *et al.*, 2005; Birgersson and Karnland, 2009; Hedström and Karnland, 2011**). In the present tests, the amount of interlayer salt was expected to increase

with increasing concentration in the surrounding solution. As the ionic concentration increased in the montmorillonite interlayer during the introduction of salt, the water activity was lowered inside the montmorillonite, changing the osmotic balance between the interlayer and the external solution in such a way that less ice was formed resulting in a higher hydration of the montmorillonite.

Salt intercalation in the montmorillonite interlayer has also been observed in several other systems, **Sposito *et al.* (1983)** claim to have found evidence for salt intercalation in Wyoming montmorillonite by investigating the difference between uptake of chloride and perchlorate salts. **Ferrage *et al.* (2005)** found support for salt intercalation in the montmorillonite interlayer by preparing Ca-montmorillonite samples from deionized water and water containing salt. In X-ray diffraction measurements the basal spacing of the dried sample was changed to higher spacings in the sample prepared in salt solution, indicating a change in the interlayer composition. **Karnland *et al.* (2005)** drew similar conclusions when comparing experimental swelling pressure data with model calculations of confined Na-montmorillonite in contact with 0-3 M NaCl solutions. The model suggested that the measured swelling pressures could only be explained by introducing Na^+ and Cl^- from the salt solution to the interlayer space of the montmorillonite, hence changing the osmotic equilibrium by lowering the water activity in the interlayer water in relation to the external solution. The number of ions entering was quantitatively described by the Donnan equation.

In parallel with the formation of ice, hydrohalite ($NaCl \cdot 2H_2O$) was formed in the Na-case (**Figure 25c**) and in the Ca-case the salt hydrate phase antarcticite ($CaCl_2 \cdot 6\ H_2O$) was sporadically formed (**Figure 25c**). It seems that the salt at low temperature (e.g. -50 ºC) may either remain as hydrated interlayer ions, causing expanded montmorillonite (Ca-case), or the ions could leave the interlayer and form the salt hydrate on the outside, contracting the montmorillonite (Na-case). Most antarcticite was formed at 0.5 M $CaCl_2$, were the montmorillonite was not as fully expanded as at higher concentrations. At 2.5 M minor antarticite was formed and seemed to correlate with a minor dip in the basal spacing (**Figure 25b**). The formed hydrohalite was lowest at 1 M NaCl and it was also at this concentration where the basal spacing had its maximum (**Figure 25a**).

Summary

Salt, especially calcium chloride, may dramatically reduce the montmorillonite dehydration at freezing temperatures (< 0 ºC). This was interpreted as a consequence of salt intercalating the interlayers.

Swelling of smectite with liquid ethylene glycol in time and space

Time-resolved swelling of oriented smectite films

Oriented films were prepared from Mg-IbecoSeal smectite clay (Askana region, Georgia) as W0, W1, W2 and W3 hydrates (**Svensson and Hansen, 2010a**). The films were approximately 65 µm thick and a drop of liquid ethylene glycol was placed on the film and the intercalation was monitored with time using X-ray diffraction. The intercalation was followed by the gradual intensity increase of the 17 Å peaks (**Figure 26**) corresponding to the smectite glycolate whereas the hydrate peak intensity gradually decreased in a rather symmetric manner (one example is presented in **Figure 26b**). No relation could be seen between the intercalation time and the hydration stage (W0 – W3) of the smectite film. The effect of inhomogeneity in the film (thickness/quality) was likely much larger than the effect of the water content. The rate of the reaction was shown to be linearly related to $time^{1/2}$ (**Figure 26c**) which is compatible with diffusion control (**Fisher, 1978; Crank, 1980**) or a capillary-controlled process (**Lucas, 1918; Washburn, 1921**). Effective diffusion coefficients were calculated as $D = 2x^2/t_f$, where x is the thickness of the smectite film and t_f is the time of complete intercalation (**Crank, 1980**). Coefficients for the different experiments were in the order of $D = 10^{-11}$ m^2/s. The diffusion coefficients were compared with coefficients for water in smectite and vermiculite, ethylene glycol and propylene glycol in vermiculite and poly ethylene glycol in smectite and vermiculite. Generally the diffusion coefficients are higher in vermiculite than in smectite and lower for ethylene glycol compared with water. If the experiment could be performed with well-defined smectite films, it could be a convenient way of determining diffusion constants of the various liquids that can intercalate smectite clay. As the glycolation proceeded the hydrate basal spacing was seen to increase (**Figure 26d**). This was interpreted as a redistribution of water in the sample.

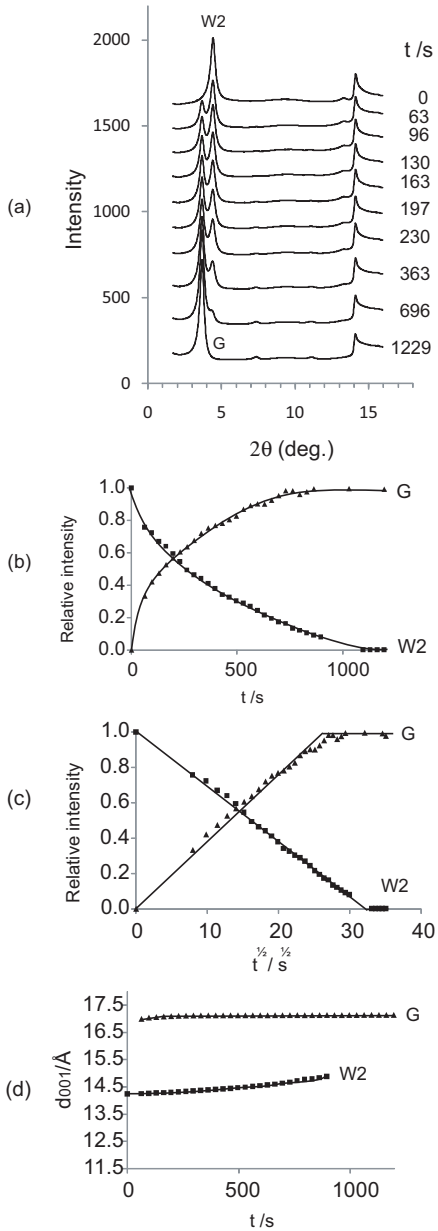

Figure 26. Glycolation of an oriented Mg-smectite W2 film (IbecoSeal) resolved in time. (a) A selection of integrated diffractograms, (b) the relative intensity of the smectite hydrate and glycolate as a function of time, (c) the relative intensity of the smectite hydrate and glycolate as a function of the square root of time, (d) the basal distance of the smectite hydrate and glycolate as a function of time (**Svensson and Hansen, 2010a**).

Time and spatially resolved swelling of smectite powder in capillary

Dialyzed and homoionic (Li^+, Na^+, K^+, Mg^{2+}, Ca^{2+}) powder of Wyoming montmorillonite was packed in glass capillaries and liquid ethylene glycol was added to one end of each capillary (**Svensson and Hansen, 2010a**). The saturation was allowed to proceed for up to 19 hours, and the glass capillaries (diameter = 1.5 mm) were probed at different times with a 1 x 1 mm^2 X-ray beam. The dry part contained the original bentonite and the wet part contained 17 Å-glycolate (see **Figure 27** for an example). In the dry part, in front of the wetting front, a 0.5-2 mm zone with increased basal spacing was observed in all cases, except for the K-form. The zone with increased water content contained the following hydrates: more W2 (Li); W2 (Na); W4 (21 Å) and W3 (Mg); and W3 (Ca). The water was much more volatile and had a higher diffusivity than the glycol and was transported ahead of the saturation front. Visually the glycolated smectite looked wet to the eye whereas the zone with increased water content looked exactly the same as the original smectite. A previously unreported 21 Å basal spacing was found in the Mg-Wyoming montmorillonite in the interface between pure water (19 Å) and pure ethylene glycol (17 Å). **Barshad (1952)** examined the swelling of smectite in mixtures of organic solvents (lower ε) and water. He considered that an increase in the dielectric constant (owed to the progressive addition of water to the organic solvent) decreased the Coulombic attraction between the exchangeable cations and the charged silicate sheets and thereby explained the observed expansion in the basal distance. **Brindley et al. (1969)** studied Ca-smectite swelling in organic-water mixtures and observed a similar expansion, when the mineral in pure organic solvent was compared with that in pure water. A maximum in the basal distance was observed at intermediate compositions of water and organic solvent. Most likely, this is very similar to what was observed in the case of water-glycol interface in this study.

Summary

Small amounts of water present in the glycolated smectite may impact the basal spacing, hence this should be considered when preparing such samples to avoid misinterpretations. If well-defined clay films can be prepared, time and/or spatially resolved data may fairly rapidly provide diffusion coefficients of various liquids that may intercalate the smectite layers.

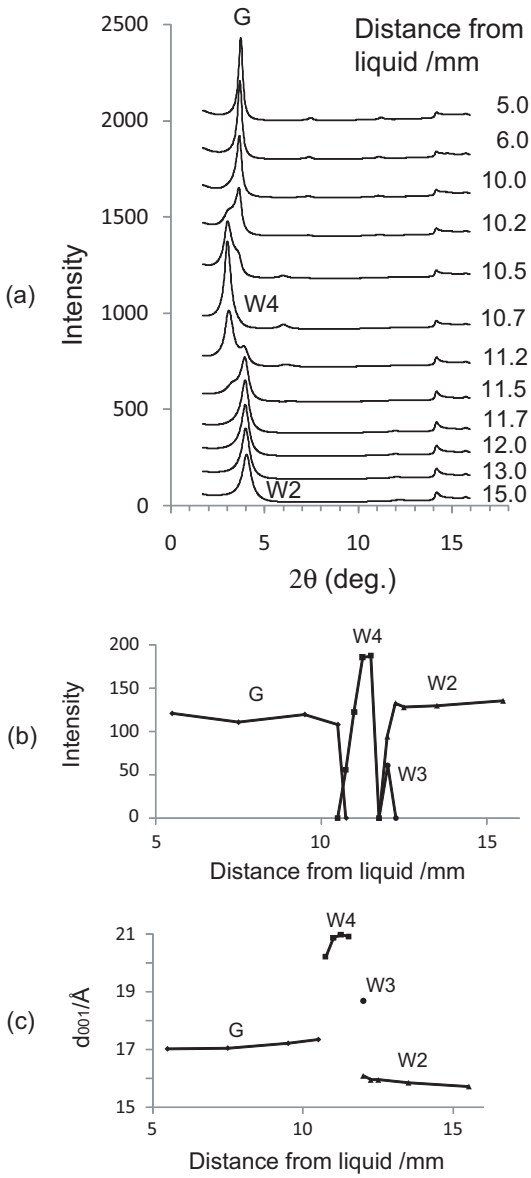

Figure 27. Spatially resolved glycolation of Mg-montmorillonite in a capillary after seven hours. (a) A selection of integrated diffractograms as a function of the distance from the pure liquid. (b) The intensity of the glycolate, W4, W3 and W2 phases as a function of the distance. (c) The basal spacing of the glycolate, W4, W3 and W2 phases as a function of the distance (**Svensson and Hansen, 2010a**).

The bentonite barrier – Fe redox chemistry in field experiments

The iron in the octahedral sheet of the montmorillonite is susceptible to redox changes caused by chemical and microbiological reactions (**Pentráková *et al.*, 2013; Zhang *et al.*, 2013**). If the Fe(III) is reduced to Fe(II) this may impact the layer charge and hence potentially several of its important properties (*e.g.* **Stucki *et al.*, 1984, 2002; Wu *et al.*, 1989**). There are indications that the octahedral iron in different smectites reduce at different reduction potentials (**Gorski *et al.*, 2013**); hence the Fe redox chemistry in smectites could be used as an indication of the reduction potential in a field experiment. When mined, bentonite normally has a variety of colors that normally change upon drying, and the color is often assumed to depend on the oxidation state of iron in the bentonite (**Figure 2**). Bentonite processing normally involves milling and drying by heating at high temperature, which most likely will oxidize any naturally reduced smectite. Bentonite is also normally investigated under aerobic conditions. Engineered barriers for radioactive waste repositories, however, provide an anaerobic or even reducing environment. At great depth the oxygen partial pressure is much lower than at the surface and the deep ground water is generally anoxic and may contain dissolved Fe(II) (**Bath and Hermansson, 2009; Grenthe *et al.*, 1992; White and Yee, 1985**). Hence, knowledge about redox changes in bentonite and how they potentially affect its properties is an important area of study. Reduced montmorillonite and many Fe(II) corrosion products are oxygen-sensitive and may oxidize rapidly in air (**Svensson and Hansen, 2013b**). Hence, sample exposure to air must be minimized by quick handling and good packaging from the point of excavation to the measurement. Larger samples are less sensitive than smaller samples (because of diffusion-limited transport of oxygen within the water-saturated samples). Hence, the final sampling should be done just before the measurements and in an anaerobic box with inert atmosphere. In the studies presented in this thesis, the larger samples were packaged as quickly as possible by vacuum sealing in aluminum-laminate bags, and at the synchrotron the bags were opened in an argon-filled glovebox for final sampling. The total time between the uptake and the analysis (**Figure 28**) was minimized as much as possible, which was not always a simple task, considering the extensive planning of the excavation of large field experiments and applying in advance for time at the synchrotron. For the ABM1 package the measurements at the synchrotron took place two and a half weeks after

the uptake and for the Prototype samples less than one week. In the case of TBT the time between excavation and measurement was longer.

Alternative Buffer Material experiment 1 (ABM1)

In ABM1 different trends were seen in different blocks (**Svensson and Hansen, 2013b**). Some profiles had a significant increase in the Fe(II)/Fe-total ratio (**Figure 28a-d**), whereas others showed no clear trend. In one case involving French Callovo-Oxfordian clay stone, originally high in Fe(II) phases, the clay was more oxidized after the experiment than before (**Figure 28f**). This was interpreted as oxidation of Fe(II)-phases such as pyrite present in the clay stone. The general increase in Fe(II) in ABM1 bentonites correlated with an increase in total iron, so it is reasonable to believe that the Fe(II) increase was owed to Fe(II) release from the corrosion of the iron heater.

The observations in ABM1 are rather similar to what has been observed in small scale laboratory experiments. **Carlson *et al.*, (2007)** found an increase in the Fe(II)/Fe-total from 36 to 75% using Mössbauer spectroscopy and total iron increase from 3 to 13 wt% in compacted MX-80 bentonite with carbon steel wires and coupons (50 ºC; 2½ years). In compacted bentonite samples (MX-80; eight years; 20 ºC) in contact with solid iron **Kumpulainen *et al.* (2010)** found an Fe(II) increase from 50 to 60% using Mössbauer spectroscopy and total iron increase from 3 to approximately 20 wt%, while the author of this thesis on the same sample found an increase from approximately 20% in reference material to 35% Fe(II)/Fe-total in exposed material, analyzed using XANES in the same way as with the ABM1-samples above.

Temperature Buffer Test (TBT)

In the bentonite samples from the TBT experiment (**Svensson and Hansen, 2013b**), no significant increase in Fe(II) content was observed (**Figure 28h**). A similar conclusion was also reached by **Åkesson *et al.* (2012)** using Mössbauer spectroscopy on similar samples from the TBT experiment. At the heater interface a magnetic Fe(III)-phase was observed, and later identified as maghemite by XRD (**Svensson and Hansen, 2013b**). The maghemite may have formed directly from the corrosion or the oxidation of magnetite that was possibly formed as an intermediate corrosion product. Magnetite may convert to maghemite at high temperature and aerobic conditions. In micron sized magnetite particles the conversion occur at approximately 220 °C and in ultrafine particles (~100 Å) the conversion may occur as low as 55 °C (**Haneda and Morrish, 1977**). Hence, the maghemite formation in TBT seems likely to have formed at high temperature

during the active phase of the field experiment, and not because of unintended post-excavation oxidation during sampling and/or later storage.

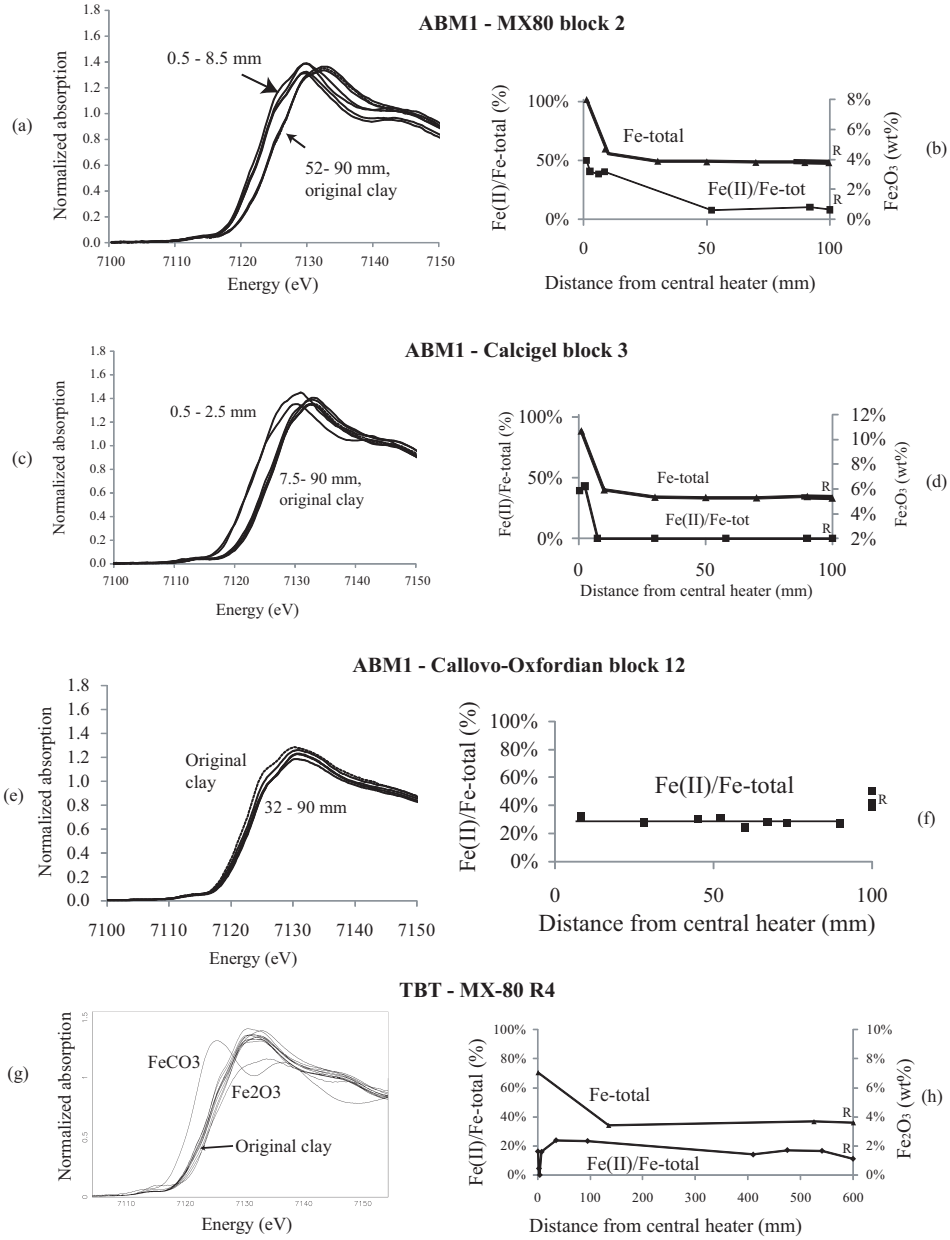

Figure 28. XANES spectra of ABM1 and TBT samples of samples and original clay. Fe(II)/Fe-total fraction (squares) and Fe_2O_3 content (triangles) are marked in the block. The reference value(s) of the original clay is located on the right and marked R (**Svensson and Hansen, 2013b**).

ABM1 - Dynamic oxidation experiments (kinetics)

Samples that were found to be rich in Fe(II) were later exposed to ambient atmospheric oxygen, and the oxidation of Fe(II) to Fe(III) was followed in-situ with time to establish the sensitivity of the samples to oxidation (cf. **Figure 29**). This gave input for the design of future sample handling procedures and also diagnostic information about the nature of the Fe(II) -compounds present, as the existence of oxygen-sensitive phases is evidence for oxygen-free conditions in the experiment. Several of the Fe(II)-rich samples from the ABM1 package exhibited substantial oxidation in air (**Figure 29**). However, the two innermost Fe(II)-rich samples of the Calcigel clay (**Figure 29**) exhibited substantial differences in oxidation behavior. The 0.5 mm sample was only somewhat oxidized from 36 to 33% in 50 minutes (**Figure 29a**). Hence, this sample included a phase that was stable to atmospheric oxygen (possibly poorly crystalline magnetite). However, the Fe(II)/Fe-total content in the 2.5 mm sample decreased from 23 to 3% in 20 minutes, indicating an oxygen-(air) sensitive Fe(II)-phase. When the Fe(II) content was plotted towards the square root of time, a linear relation was found (R^2 = 0.99). This is typical of a diffusion controlled process such as drying of the clay or diffusion of oxygen (air) and supports the statement that larger samples are much less sensitive than smaller ones, as the time for diffusion transport increased exponentially with the sample thickness.

ABM1 – COX - Statistical error estimations of the XANES method

The Callovo-Oxfordian (COX) clay stone was found to have a Fe(II) content approximately similar to the bentonites from the field experiment with the highest Fe(II) content. COX samples from the ABM1-field experiment were interpreted to have a lower Fe(II)-content than the original clay, and a number of XANES-spectra were collected to also get a lot of data for a statistical evaluation of the method (**Table 2**). As with all other samples, three consecutive scans were recorded. Instead of combining the scans before evaluation, each separate scan was evaluated and the standard deviation of the results were in the range of 0.9 to 2.4 %, while the standard deviation of the Fe(II)-content between different samples were in the range of 3.0 to 4.2% (**Table 2**). The difference in Fe(II)-content between the samples from the field experiment and the reference samples were 43% – 31%= 12%, which is about three times larger than the standard deviation of the Fe(II)-content of the samples (**Svensson and Hansen, 2013b**).

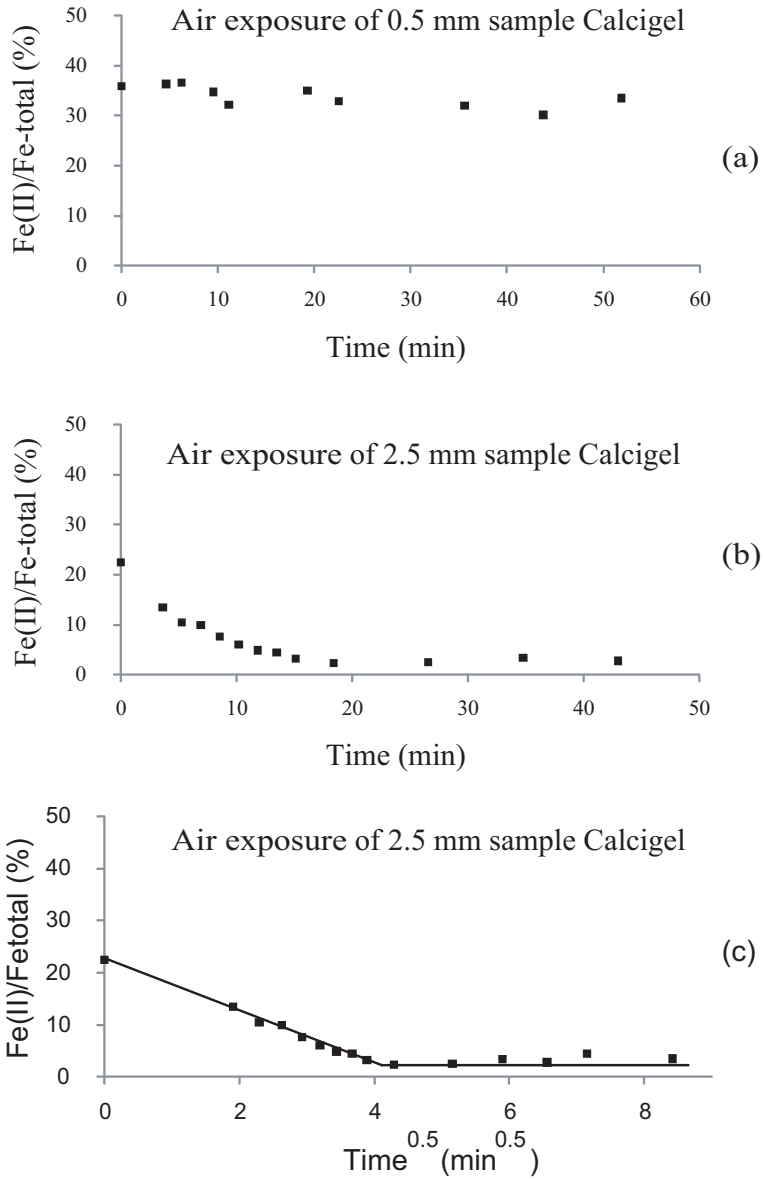

Figure 29. Oxidation of Fe(II)-rich Calcigel samples from ABM1 (block 5) by air, followed with time by XANES. Sample taken 0.5 mm from the iron heater as a function of time (a). Sample taken 2.5 mm from the iron heater as a function of (b) time, and (c) as a function of the square root of time (**Svensson and Hansen, 2013b**).

Table 2. Statistical summary of the Fe-redox measurements (XANES) of original crushed Callovo-Oxfordian (COX) clay stone and heated material from the ABM1-experiment. The variation in Fe(II)/Fe-total due to the measurement is compared to the variation due to the material composition by comparing 3 analyses of the same sample to measurements of different samples (**Svensson and Hansen, 2013b**).

Sample	**Measurement no**	**Fe(II)/Fe-total**	**Average (std dev)**
COX	1	34.2	33.2 (1.6)
32 mm from heater	2	31.3	
	3	34.0	
COX	1	32.9	33.6 (2.4)
52 mm from heater	2	31.6	
	3	36.2	
COX	1	30.1	31.0 (0.90)
67 mm from heater	2	31.1	
	3	31.8	
COX	1	28.3	27.2 (1.7)
90 mm from heater	2	25.2	
	3	28.1	
	Average (std dev):	**31.0 (3.02)**	

Sample	**Measurement no**	**Fe(II)/Fe-total**	**Average (std dev)**
COX original clay			
sample 1	1	41.6	39.7 (1.7)
	2	38.6	
	3	38.9	
COX original clay			
sample 2	1	38.9	40.6 (1.5)
	2	41.6	
	3	41.4	
COX original clay			
sample 3	1	49.1	48.1 (0.92)
	2	47.3	
	3	47.9	
	Average (std dev):	**43.0 (4.2)**	

Prototype outer section (deposition hole 6)

In the Prototype experiment the heater consisted of copper instead of iron as was the case in ABM and TBT. Hence in the Prototype experiment the contribution of any iron corrosion products could be neglected. During the excavation and sampling of the bentonite buffer, a dark discoloration of the bentonite was seen at the canister interface (~10 mm), and this discoloration disappeared irreversibly upon drying in air for two weeks (**Figure 30**). XANES data was collected for samples within the 0 to 50 mm range from the canister and indicated an increase from 21 to 48% Fe(II)/Fe-total (**Figure 31**). Another team in Finland analyzed similar samples using Mössbauer spectroscopy and found an increase from 30 to 48% Fe(II)/Fe-total (**Figure 31**; **Olsson *et al.*, 2013**).

An Fe(II) increase in an iron-bentonite experiment such as ABM1 was more or less expected, however, an increase in Fe(II) in a copper-bentonite experiment as in Prototype was rather unexpected. No previous Fe-redox studies on bentonite in contact with copper in field experiments have been found in the literature. According to both the XANES and Mössbauer data, a reduction of the iron in the bentonite seems to have occurred, and according to Mössbauer data, not only in the direct vicinity of the canister (**Svemar *et al.*, 2013**). In the XANES data the samples further out from the canister were somewhat lower in Fe(II)/Fe-total, whereas in the Mössbauer data the difference is much smaller. A maximum Fe(II)-content at the canister interface followed by a drop is also somewhat supported by the visual observations (**Figure 30**). An increase at the copper indicate that the reduction of Fe(III) to Fe(II) in the bentonite possibly could have been a redox reaction with the copper material. However, 10-20% of the iron in the bentonite seems to have been reduced. The MX-80 bentonite consist of approximately 3.5 wt% Fe_2O_3 (**Karnland *et al.* 2006**). The weight of one bentonite block in the experiment was ~ 2000 kg. Hence, in every single block of bentonite 7 to 14 kg of Fe(II) was produced, whereas only 100 ppm of copper was observed in the innermost 5 mm. This amount of copper cannot have reduced 7 to 14 kg of Fe(III) based on the mass-balance relation, hence it seems very unlikely that the copper metal worked as a reductant. It has been observed that the Fe- redox chemistry in different smectites are affected differently by the external redox potential (**Gorski et al. 2013**). Both XANES and Mössbauer spectroscopy indicated approximately 50% Fe(II)/Fe-total in the bentonite at the canister interface (**Figure 31**). According to **Gorski et al. (2013)** this Fe(II)/Fe-total ratio correspond to a redox potential of approximately -50 mV SHE for Wyoming montmorillonite. This is very close to the potential measured on three installed copper electrodes in the bentonite inside the Prototype experiment (dh5) that showed values in the range of -60 to -30 mV SHE (**Rosborg, 2013**). Hence it seems that the montmorillonite in the bentonite might have adapted to the

surrounding redox conditions. The gradient towards the canister could possibly be due to the thermal gradient affecting the kinetics of the Fe(III) reduction, or possibly the copper surface distributed the electrons, however being rather inert in itself.

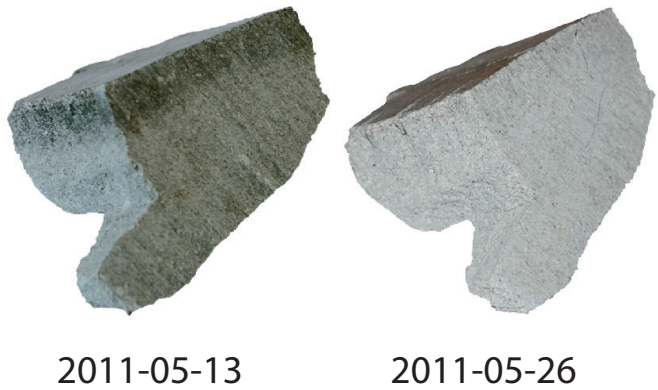

Figure 30. Bentonite sample from Prototype deposition hole 6, ring 10. Visual effect from drying in air for approximately two weeks.

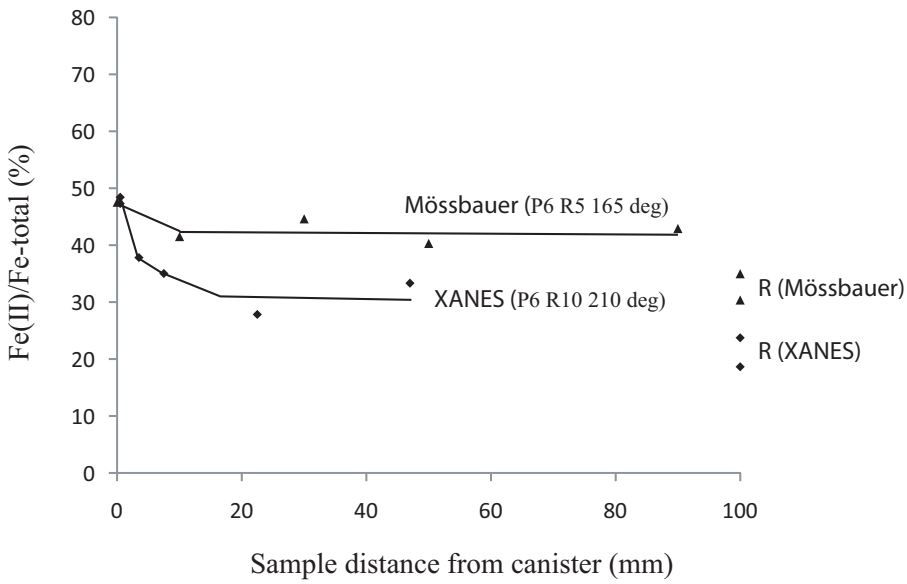

Figure 31. Fe(II)/Fe-total as determined by XANES (Svensson and Hansen) and Mössbauer spectroscopy (Lindén, Åbo Akademi, Finland) of samples from Prototype deposition hole 6. R = reference samples. (**Olsson *et al.*, 2013**).

Summary

Based on the changes in Fe(II)/Fe(III) and/or observation of oxygen-sensitive phases, one iron-bentonite experiment (ABM1) and one copper-bentonite experiment (Prototype) were interpreted to have reached reducing of partly reducing conditions in relation to the Fe(III) in bentonite, while one experiment was found to still be in more oxidizing conditions (TBT). Most likely the size of the experiments, the availability of water, the temperature, the heater material and the total experiment time, all had an impact on the oxygen consumption. The TBT experiment also contained parts with sand, and sand has a relatively large amount of initial porosity (installed air) compared to compacted bentonite. The relatively high temperature needed to form maghemite (**Haneda and Morrish, 1977**) indicate that the high Fe(III)/Fe(II) ratio in the TBT samples most likely was not due to unintended oxidation during or after the excavation of the experiment. Field experiments are very complex with plenty of installed electrical cables etc, and it is possible that this may have affected the results. Further information about the reduction of Fe(III) in montmorillonite and about the properties of partly and/or fully reduced montmorillonite would be valuable.

The bentonite barrier - Mineral evolution

As the designed repository lifetime is extremely long (0.1 to 1 Ma), it is of the highest importance that the smectite minerals do not transform over time into non-swelling minerals to such an extent that the performance of the buffer degrades. One rather common, but extremely slow, transformation reaction found in nature is the transformation of montmorillonite to illite, *i.e.* illitization (**Arthur *et al.*, 2005; Karnland and Birgersson, 2006**). The illitization is assumed to depend strongly on the thermal conditions and the availability of potassium. Many natural analogs for this process exists and has been used as a complement to experimental data from short-term laboratory experiments, one beeing in Kinnekulle, Sweden (**Pusch and Madsen, 1995**). Smectite illitization has also been argued to have microbiological pathways (**Zhang *et al.*, 2007; Liu *et al.*, 2012**). One of the most important methods for studying illitization of montmorillonite is XRD and ethylene glycol intercalation, as studied in **Svensson and Hansen (2010a)**.

The introduction of potentially reactive construction material such as metallic iron or concrete means other potentially harmful reactions may occur. Cement-leaching water may have a very high pH that can dissolve or react with bentonite. This has been studied as a natural analog project in Cyprus, where bentonite can be found in contact with naturally alkaline waters (**Alexander *et al.*, 2011**). On the inside of the KBS-3 copper canister there is an iron insert, and iron is also planned for use in rock reinforcements. The metallic iron is thermodynamically not stable in the repository and the interaction between corroding metallic iron and bentonite has recently been studied by several researchers (**Guillaume *et al.*, 2004; Lantenois *et al.*, 2005; Charpentier *et al.*, 2006; Carlson *et al.*, 2007; Perronnet *et al.*, 2008; Wersin *et al.*, 2008**). Metallic iron could affect the buffer in several ways: (1) reduction of Fe(III) to Fe(II) in montmorillonite, potentially affecting the clay mineral layer charge, (2) dissolution and/or alteration of montmorillonite to another mineral and (3) cementation of the bentonite by corrosion products affecting the plasticity, hydraulic conductivity and/or swelling ability.

Montmorillonite has been found to be either stable or in some cases to convert to Fe-rich trioctahedral smectite, Fe-serpentine, chlorite, or vermiculite, depending on the temperature and experimental conditions. Factors such as the density and

liquid/solid ratio, temperature and pH seem to be important for predicting the outcome of an iron-bentonite experiment. The more the experiments mimic the true technical application, the more the results are likely to be suitable for a specific application. All bentonite buffers in high-level radioactive waste repositories are of compacted bentonite with a low liquid/solid ratio, and most of the studies performed showing alteration products have been conducted at high liquid/solid ratio in non-compacted systems. When it comes to mineral evolution, the focus in this thesis has been on the formation of trioctahedral clay minerals in Äspö field experiments.

Formation of trioctahedral clays minerals in Äspö field experiments

A variety of newly formed phases has been seen in the different field experiments investigated during the work of this thesis. In TBT a magnetic Fe(III) phase was identified as maghemite in the close vicinity of the iron heater (**Svensson and Hansen, 2013b**). In the investigated Prototype samples a white precipitate in the vicinity of the copper canister was identified as gypsum (**Olsson *et al.*, 2013**). In ABM2, centrosymmetrical precipitates were seen in several blocks (**Figure 32**), typically consisting of Ca-sulphates and carbonates. These processes were expected and are relatively well understood (**Karnland *et al.*, 2009; Dueck *et al.*, 2011**). The presence of water-soluble Ca-minerals such as gypsum in the bentonite buffer has been regarded as potentially beneficial to some extent (**Liu and Neretnieks, 2006**).

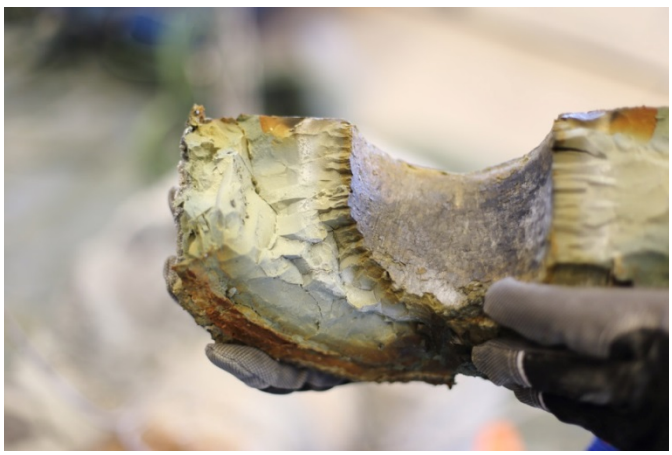

Figure 32. Excavated bentonite sample of Deponit CA-N from the ABM2-experiment. Visually dark corrosion products at the heater interface and white centrosymmetrical precipitates some centimeters away can be observed.

However, less expected was the appearance of newly formed trioctahedral phases that were observed in some of the innermost samples closest to the iron heater in ABM1 and TBT (**Svensson and Hansen, 2013b**; **Figure 33**). Dioctahedral smectites (such as montmorillonites) have a 060 reflection at 1.50 Å, whereas trioctahedral smectites (such as saponite) have a 060 reflection at about 1.52 Å but, apart from that, seems to have rather similar properties.

Alternative Buffer Material experiment 1 (ABM1)

Kaufhold *et al.* (2013) found a change in the 060 region in several ABM1 samples (blocks: Febex #8, MX80 #11 and Ikosorb #10) and correlated this with an increase in total MgO and a trioctahedral band in the infrared spectroscopy (FT IR) data, whereas other ABM1 clays such as Rokle remained unchanged. Trioctahedral smectites are generally high in Mg and Fe(II), whereas dioctahedral smectites are generally high in Al and/or Fe(III), and minor Mg. Hence, formation of trioctahedral smectites is expected also to correlate with a change in the chemistry. **Svensson and Hansen (2013b)** found similar changes in ABM1 blocks Calcigel #5, but found block MX80 #2 unaffected. Hence, the changes were not only different for different clays, but the same clay behaved differently depending on its position in the experimental package.

Temperature Buffer Test (TBT)

Åkesson *et al.* (2012) found a broad and diffuse increase in the background in the 060 region in samples taken from the iron heater interface in the TBT experiment. In **Svensson and Hansen (2013b)**, a broad reflection at approximately 1.52 Å was found in similar samples from the TBT experiment and was associated with what seems to be formation of a trioctahedral clay mineral (**Figure 33**).

Prototype outer section (deposition hole 6)

In experiments with copper heaters no trioctahedral phases were observed in the Prototype field test at Äspö (*e.g.* **Figure 33d; Olsson et al., 2013**). However, a minor increase in the MgO content without correlation with a new phase in the XRD data was observed both in Prototype (**Olsson *et al.*, 2013**) and also in other field experiments with copper (*e.g.* **Karnland *et al.*, 2009**). A minor formation of a few mass percent of trioctahedral Mg-smectite in the innermost 2 mm from the heater could be the explanation for the minor increase in MgO; however, the level is definitely below that which is possible to detect with current XRD data (**Svemar *et al.*, 2013**).

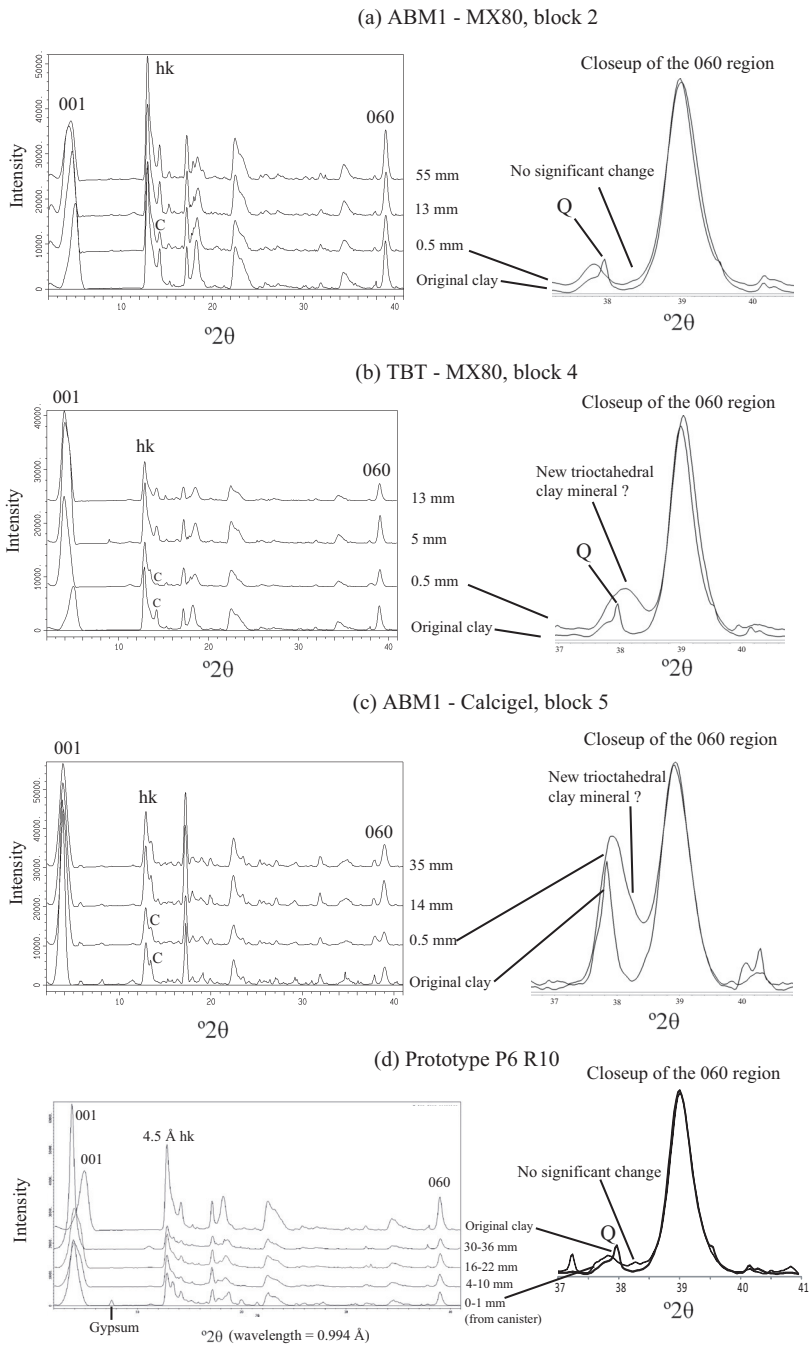

Figure 33. XRD data from ABM1 (MX80 block 2, Calcigel block 5), TBT (MX-80) and Prototype (MX-80) with a closeup of the 060 region. λ = 0.994 Å. (a-c, **Svensson and Hansen, 2013b**; d, **Olsson et al. 2013**).

The following section is based purely on unpublished results by D. Svensson

The data in this section was not collected at MAX-lab but instead at the new laboratory facilities at Äspö Hard Rock Laboratory, Oskarshamn, Sweden. The XRD data was collected in reflection mode (theta-theta configuration) using a Panalytical X´Pert Pro system with a Co X-ray source (broad focus; λ = 1.789 Å), a PIXcel1D linear detector and programmable divergency- and anti-scatter slits. In order to maximize the intensity no monochromator was used, however a thin Fe filter was used for suppression of white- and Co K-beta radiation, making the K-beta intensity <1% of the K-alpha. The samples were either back-loaded or prepared on a zero-background Si substrate, depending on the amount of sample available. Data collection was done for typically 1-3 hours per sample at 40 kV and 40 mA. The XRF data was collected with a Panalytical Epsilon 3 XL using the included Panalytical Omnian standard method for quantifications. Helium gas was flowed over the sample during the measurement to reduce the absorption by the air, and the samples were analyzed as compacted discs.

Alternative Buffer Material experiment 2 (ABM2)

Much higher content of trioctahedral smectite was found in samples from the ABM2 experiment compared to ABM1 and TBT (**Svensson, 2013**). One sample was taken by scraping corrosion products directly from the heater at Febex block number 9. This sample was found to be composed of a mixture of magnetite from the corrosion, the original bentonite and what was identified to be a newly formed trioctahedral smectite (**Figure 34**).

The scraping sample from the iron heater – Febex bentonite interface was dispersed in water and the magnetite was separated with a magnet. The non-magnetic fraction was cation-exchanged into Ca-form, in order to separate interlayer Mg from Mg in the smectite octahedral sheet in the chemical data. Saturation with ethylene glycol gave a basal spacing of ~17 Å and no other reflections could be seen in the low angle region corresponding to any other clay mineral. Due to the very low amount of sample (~100 mg), the quality of the dataset was far from optimal and no further detailed evaluation of the position of the 002 and 003 reflections was performed. Based on the intensity relation between the 060 reflections a rough estimate of the dioctahedral to trioctaheral smectite ratio in the sample was 60:40 (**Figure 34b**). XRD analysis of the entire Febex # 9 profile was performed and the trioctahedral phase was only seen in the innermost 0 to 2 mm closest to the iron heater (**Figure 35**).

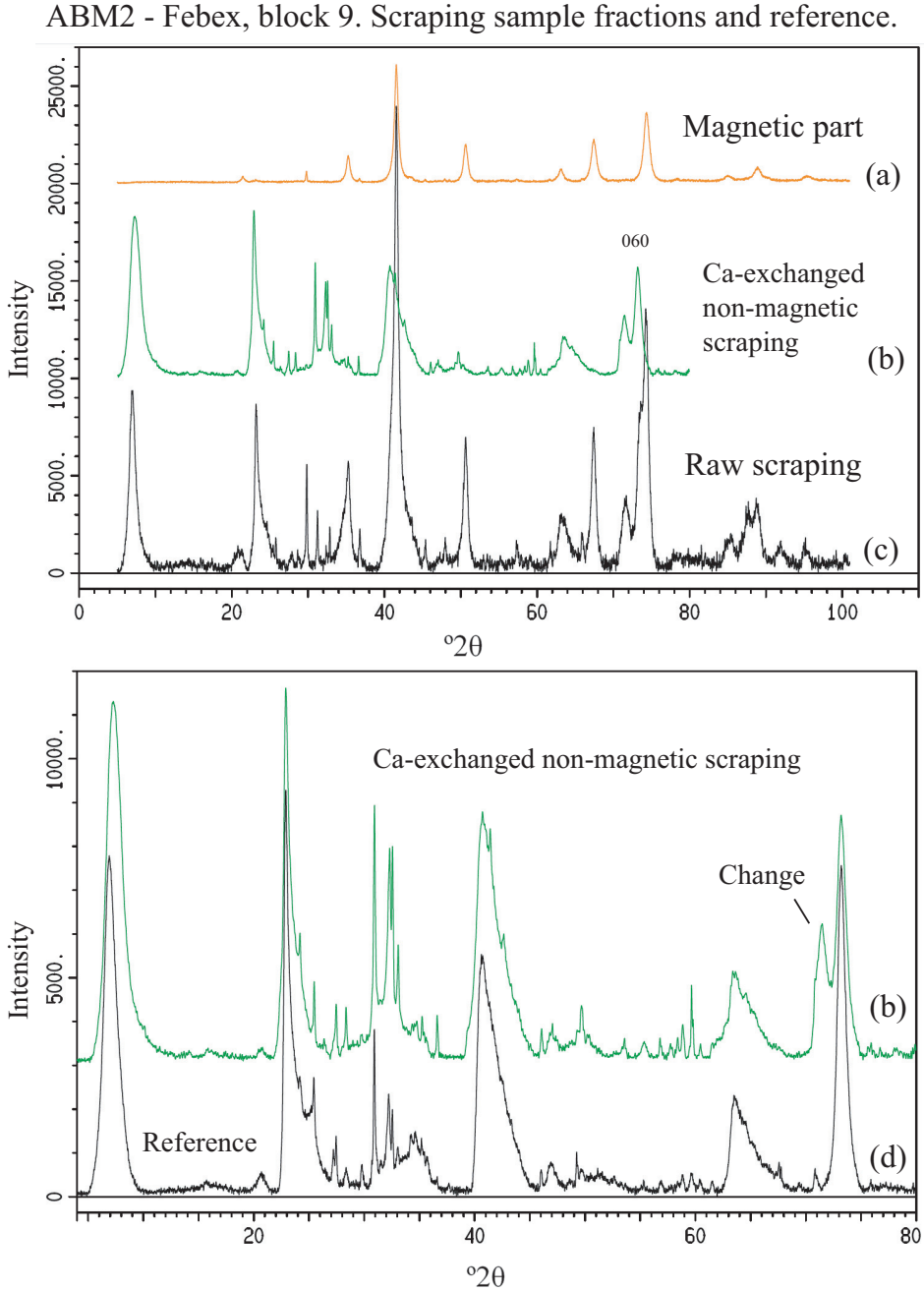

Figure 34. XRD data from ABM2, Febex, block 9. (a) Magnetic fraction of scraping sample (magnetite), (b) Ca-exchanged non-magnetic fraction of scraping sample, (c) raw scraping sample, (d) reference Febex bentonite. λ = 1.789 Å. **Svensson (2013)**.

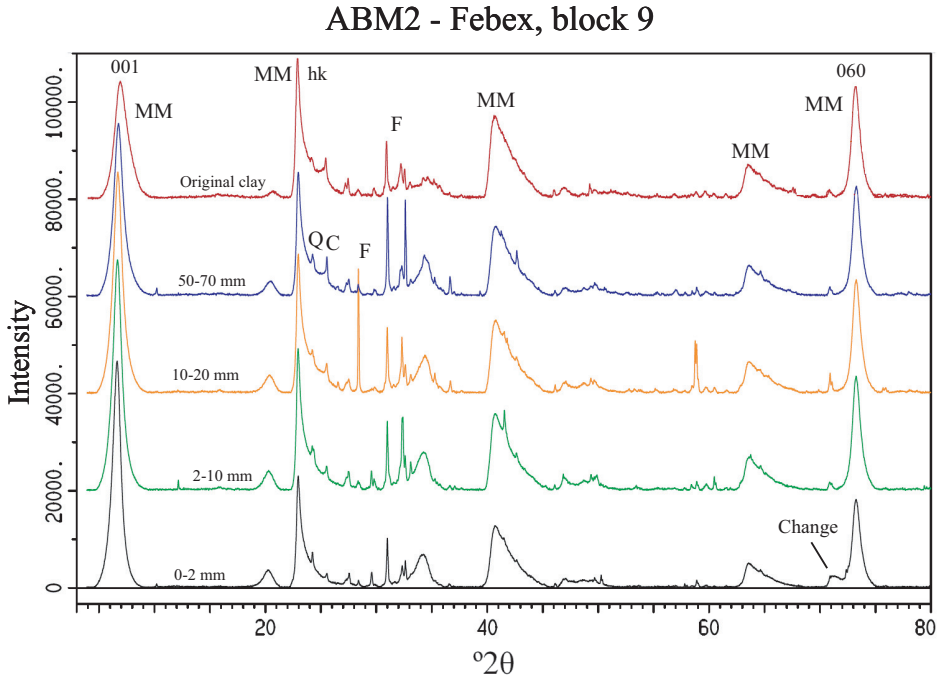

Figure 35. Powder XRD of samples from ABM2, Febex, block 9. The distance from the iron heater is given. MM= montmorillonite, Q = quartz, C = cristobalite and F = feldspar. λ = 1.789 Å. Svensson, 2014, unpublished results.

A significant increase was seen in the MgO content in the non-magnetic fraction (7.5 wt%) compared with the original bentonite (4.9 wt%; **Figure 36; Table 3 and 4**). Also, the Fe_2O_3 content increased from 4.5% in the original clay to 8.2% in the sample taken at 0 to 2 mm from the heater, 20.4% in the scraping sample from the heater (including magnetite) and 16.6% in the non-magnetic (after magnetite removal) and Ca-exchanged fraction (**Figure 36; Table 3 and 4**). The CaO content in the entire profile in the field test increased, interpreted as a result of cation exchange reaction with the Äspö ground water and/or surrounding bentonite blocks. The mineralogical content of the purified sample was estimated with the rietveld Siroquant software (CSIRO, version 3) using the XRD data. The background was manually reduced and the remaining background was refined using six coefficients and the standard algorithm of the software. For the smectite, the unit cell, the preferred orientation and the peak shape were refined. The estimated content was: 91 wt% smectite, 6.5% albite and 2.5% quartz. The difference between the data and the calculated pattern was expressed by the software as error of fit parameters for the different phases, and was in the range of 0.06 to 0.2%.

In an attempt to estimate the chemical content of the new trioctahedral phase, the chemical contribution of the identified accessory minerals and the estimated content of the original dioctahedral smectite (based on the 060 intensity relation) were subtracted from the measured elemental composition of the Ca-exchanged non-magnetic fraction of the scraping sample (**Table 4**). The ratio between dioctahedral to trioctahedral was varied slightly in order to obtain an (Mg+Fe)/(Al+Si) ratio close to 0.75, which is the ideal theoretical value for a trioctahedral smectite. This was attained with a 52.5% dioctahedral smectite and 38.5% trioctahedral smectite (58:42 ratio, very close to the 60:40 estimated from the 060 intensity relations). As the reference Febex clay fraction was Na saturated a theoretical Ca contribution was calculated from the Na content using a factor of 0.5x. The estimated chemical composition of the trioctahedral smectite corresponded to: $Ca_{1.43}$ ($Mg_{3.26}$ $Fe_{2.73}$) ($Si_{6.96}$ $Al_{1.03}$) $O_{20}(OH)_4$ (assuming Al+Si = 8). In relation to the rough approximations utilized, this fitted well with an iron rich saponite. The Ca-content indicate a somewhat higher charge -1.43 than the calculated charge from the formula -1.03. However, minor amounts of gypsum (undetected by XRD) also seem to possibly be present as 0.5 wt% SO_3 was measured. Assigning this SO_3 to gypsum indicate approximately 1 wt% of gypsum. After removing corresponding Ca from 1 wt% gypsum the estimated formula become: $Ca_{1.25}$ ($Mg_{3.26}$ $Fe_{2.73}$) ($Si_{6.96}$ $Al_{1.03}$) $O_{20}(OH)_4$, which fits somewhat better. The remaining difference reflects the uncertainties in the measurements and the approximations of the calculations. Possibly minor Ca-carbonate could also be present that explain the small remaining difference. However, both the lower and the higher charge are within the range documented for saponites, where the silicon atoms are isomorphously substituted by aluminum atoms in the interval from $Si_{7.4}$ $Al_{0.6}$ to $Si_{6.2}$ $Al_{1.8}$ (**Číčel *et al.*, 1981**).

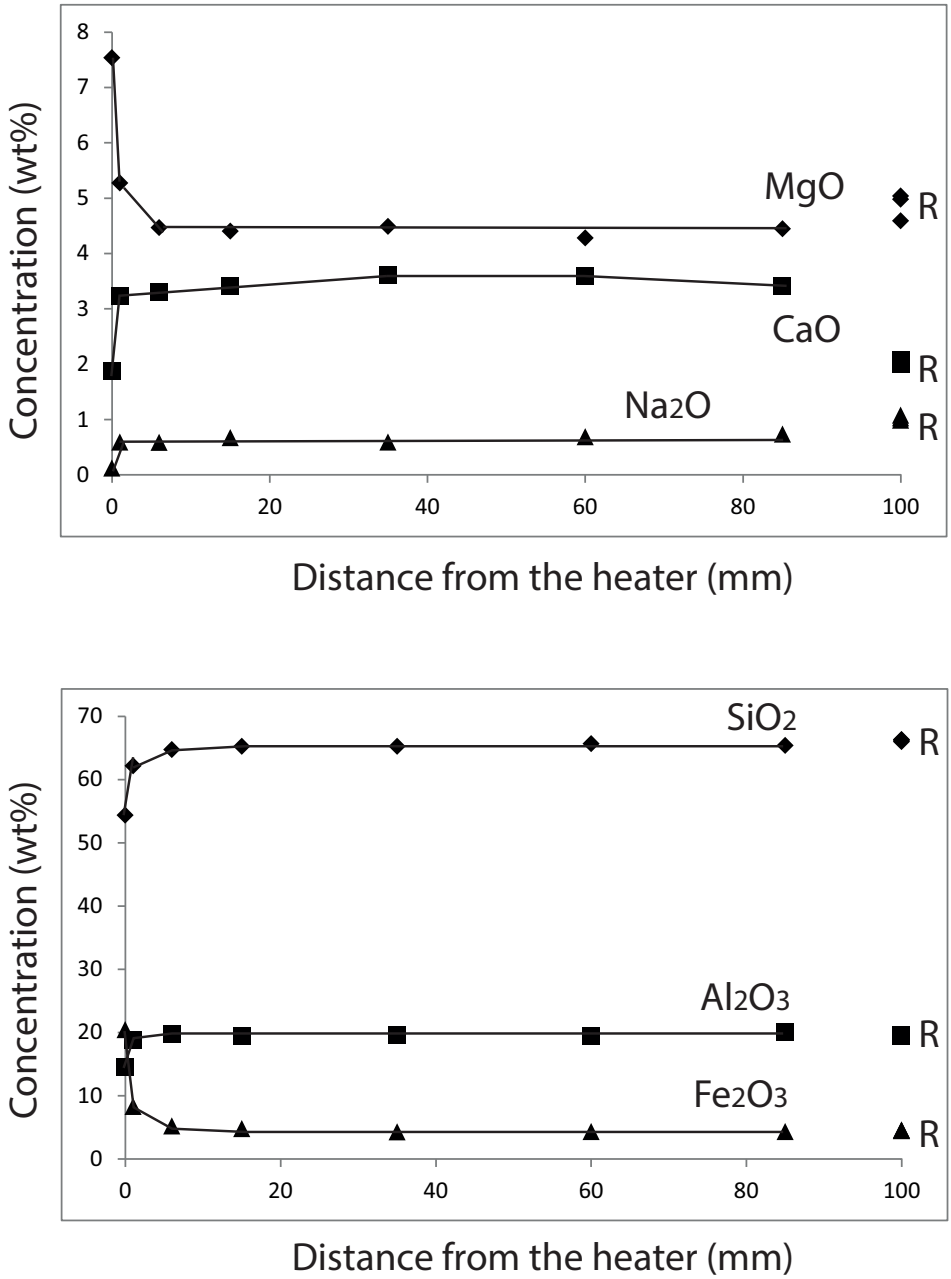

Figure 36. Elemental composition (XRF) for ABM2, Febex, block 9, and reference values (R). Svensson, 2014, unpublished results.

Table 3. Elemental composition (wt%) for the ABM2, Febex, block 9 profile and reference samples. Analyzed with XRF. Scraping concern untreated sample. Svensson, 2014, unpublished results.

Sample	Na_2O	MgO	Al_2O_3	SiO_2	K_2O	CaO	TiO_2	Fe_2O_3
Scraping	0.12	7.54	14.51	54.33	0.73	1.88	0.20	20.4
0-2 mm	0.59	5.27	18.87	62.09	0.82	3.23	0.22	8.26
2-10 mm	0.59	4.47	19.75	64.68	1.11	3.30	0.22	5.19
10-20 mm	0.67	4.41	19.52	65.19	1.19	3.42	0.24	4.74
20-50 mm	0.59	4.49	19.61	65.20	1.14	3.60	0.22	4.25
50-70 mm	0.69	4.28	19.44	65.59	1.36	3.59	0.24	4.27
70-100 mm	0.74	4.45	20.05	65.32	1.11	3.41	0.22	4.30
Reference 1	0.99	4.98	19.41	66.19	1.34	2.06	0.24	4.53
Reference 2	1.08	4.59	19.63	66.26	1.31	2.08	0.23	4.44
Reference 3	1.03	5.04	19.62	65.93	1.37	2.00	0.25	4.52
Average:	1.03	4.87	19.55	66.12	1.33	2.05	0.24	4.50
Std deviation:	0.04	0.25	0.13	0.18	0.02	0.04	0.01	0.05

Table 4. Estimation of the chemical content of the trioctahedral smectite in ABM2 Febex block 9 by subtraction of known components of the total composition. Scraping sample concern the non-magnetic and Ca-exchanged part. Svensson, 2014, unpublished results.

Sample	Wt%	MgO	Al_2O_3	SiO_2	Fe_2O_3	SO_3	K_2O	CaO	Na_2O
Scraping Ca-exch.		6.8	15.8	55.2	16.6	0.5	0.8	3.5	0.0
Febex montm.		4.8	21.0	65.9	4.3	0.0	0.6	0.1	3.1
Accessory minerals									
Quartz (SiO_2)				100					
Albite ($NaAlSi_3O_8$)			20.4	67.4					
Phase comp. (XRD)									
Febex montm.	52.5	2.5	11.0	34.6	2.2			0.8	
Quartz (SiO_2)	2.5			2.5					
Albite ($NaAlSi_3O_8$)	6.5		1.3	4.4					
The remainings:	38.5	4.3	3.4	13.7	14.3			2.6	
Sum:	100								

There are mainly two possible pathways for formation of saponite: (1) solid- state transformation of montmorillonite and (2) dissolution of montmorillonite and/or other phases followed by precipitation. **Arthur *et al.* (2005)** discuss the possibility of solid-state conversion of montmorillonite to other smectites such as beidellite or saponite because of very slow isomorphic substitution of the content in the montmorillonite octahedral and tetrahedral sheets involving Mg, Fe, Al and Si from the dissolution of accessory phases. Synthesis of trioctahedral smectites at similar conditions in the laboratory are, however, fairly straight-forward, especially at high pH, supporting the dissolution-precipitation mechanism. Synthetic saponites have been prepared at atmospheric pressure and 90 °C within 20 hours (**Vogels *et al.*, 2005**), and saponite was synthesized at 100 °C in seven days by **Kuchta and Fajnor (1987)**. Stevensite, which is a pure Mg- trioctahedral smectite (iron-free), has been synthesized by a hydrothermal reaction of amorphous silica and magnesium carbonate in basic conditions and 100 °C in 0.5 to 20 hours (**Ogawa *et al.* 1991**). Possibly dissolution of accessory phases such as cristobalite and available interlayer-Mg^{2+} and Fe^{2+} from the corroding iron may form trioctahedral smectite even without a contribution from montmorillonite dissolution.

Hover *et al.* (1999) states that formation of authigenic trioctahedral smectite is common in evaporative lake sediments, and their data indicates that dioctahedral smectite may transform to trioctahedral Mg-smectite in hypersaline porewaters with a high Mg^{2+}/Ca^{2+} ratio. **Wilson *et al.* 2006** conclude on the basis of thermodynamic considerations that, given the redox potential likely to occur in a repository, montmorillonite is more likely to transform into Fe(II)-saponite than nontronite, and that the two most likely montmorillonite alteration products are Fe(II)-saponite and berthierine. Fe(II)-saponite is expected to be favored over berthierine at high $SiO_{2(aq)}$ activity, assuming the water is saturated with respect to magnetite. **Mosser-Ruck (2010)** summarizes a number of iron-bentonite interaction studies and concludes that Fe-rich 1:1 serpentines (*e.g.* berthierine), trioctahedral smectites and trioctahedral chlorites have been observed as alteration products, and magnetite is formed as a by- product in almost all cases. The serpentine formation was favoured by high liquid/clay and by high iron/clay ratios, and the chlorite formation was favoured by a high reaction temperature.

Knowledge from laboratory synthesis, natural analogues from hypersaline marine sediments, theoretical considerations based on thermodynamics and previous small scale iron-bentonite laboratory studies support the above interpretation that ferrous saponite was formed in the ABM2 field experiment analyzed here.

The increase in the Fe(II)/Fe(III) and Fe-total (wt%) was not equal in the different blocks in the ABM1 experiment (**Svensson and Hansen, 2013b**) and **Wilson *et al.* (2006)** and illustrate the importance of high Fe^{2+} activity and low oxygen fugacity for Fe-saponite and magnetite formation. Most likely, the heterogeneity in Fe-corrosion and in the evolution of reducing conditions in the field experiments were correlated with the heterogeneity of the formation of trioctahedral Fe-smectite such as ferrous saponite in the ABM2 experiment.

Summary

Formation of small amounts of trioctahedral smectite(s) were identified in the investigated iron-bentonite field tests in the vicinity of the corroding iron. The level of formation is currently not expected to have any significant impact on the buffer performance. In experiments with copper, no trioctahedral smectites were observed. **Pusch (2001)** concludes that both montmorillonite and saponite are possible buffer candidates and commercially available in large quantities, however also states that there could be differences in *e.g.* swelling pressure at a given density. Further information about the formation of trioctahedral smectites and about their properties would be valuable, even though the impact on buffer performance with current knowledge is expected to be insignificant.

Summary and concluding remarks

In the introduction it was highlighted that calcium montmorillonite swells more than sodium montmorillonite, when equilibrated to the ambient atmosphere, whereas the direct opposite happens in liquid water, which is perhaps not particularly intuitive. Several observations, also not always particularly intuitive, have been made in the work of this thesis:

(1) Magnesium montmorillonite in water has a basal distance of 19 Å and in ethylene glycol one of 17 Å. In a gradient of ethylene glycol and montmorillonite equilibrated to ambient atmosphere, a 21 Å basal distance was identified. This may have implications for how to perform ethylene glycol solvation, which is one of the most important methods for studying smectite-illite transformation (**Svensson and Hansen, 2010a**).

(2) Calcium montmorillonite in water at room temperature has a basal distance of 19 Å and in ice at -50 °C a distance of 16 Å. Somewhere in between, before the ice formation has begun it exhibits a maximum basal distance of ~21 Å (**Svensson and Hansen, 2010b**).

(3) The basal spacing of Ca-Wyoming montmorillonite at 20 °C and 1½ - 3M $CaCl_2$ is 16 Å; however, at -50 and -100 °C it expanded to 18 Å, whereas at 0 M it dehydrated from 19 to 16 Å at a similar temperature decrease. Dissolved salts are expected to reduce the effect from freezing of bentonite in repositories compared with what would be the case with deionized water, which has been used in previous studies (**Svensson and Hansen, 2013a**).

(4) The crystalline swelling in solution has been found generally to increase with decreased temperature (until ice formation), and literature data show that osmotic swelling on the other hand increases with increasing temperature (**Hansen *et al.*, 2012**). Hence, crystalline and the osmotic swelling of smectites in water are affected differently by temperature changes.

(5) At low temperatures (-50 and -100 ºC) Na-Wyoming montmorillonite with NaCl formed salthydrate hydrohalite, whereas in the Ca-case very rarely did antarcticite form, instead the hydrated salt ions stayed in the interlayer space (**Svensson and Hansen, 2013a**).

(6) The opportunity for a divalent cation montmorillonite to expand beyond 19 Å varied with the type of montmorillonite, seemingly linked to the layer charge size and/or distribution (**Svensson and Hansen, 2014**).

(7) Zn-, and Cu- Wyoming montmorillonite exist as mixed W3 and W4 hydrates at 20 °C whereas Ca-, and Sr- montmorillonite become so at 4 °C. A general correlation was seen between the maximum swelling and the Gibbs hydration energy of the interlayer cation (**Svensson and Hansen, 2014**).

(8) Heterogeneous swelling in montmorillonite with equal access to water indicates a heterogeneity in ability to swell, and probably a heterogeneity in layer charge (**Svensson and Hansen, 2014**).

(9) In the ABM1 experiment excavated at Äspö, oxygen-sensitive Fe(II) rich phases were detected. In the TBT experiment only Fe(III) corrosion products were found. This indicated that ABM reached much more reducing conditions compared to the TBT experiment. Most likely this was due to the difference in scale, temperature and water access (**Svensson and Hansen, 2013b**).

(10) In the Prototype experiment an increase in the Fe(II)/Fe-total ratio were detected in contact with the copper canister compared with the reference material. With no increase in total iron content, this indicates a possible reduction of Fe(III) to Fe(II) in the montmorillonite, and would in that case be an indicator of somewhat reducing conditions in the final stage of the experiment in relation to the Fe(III) in the montmorillonite (**Olsson et al., 2013**).

(11) In the ABM1+2 and TBT experiments (iron heater) traces of newly formed trioctahedral clay minerals were observed. In ABM2 this phase was identified as Fe-rich saponite. In the Prototype experiment (copper heater) no trioctahedral smectites were observed.

Acknowledgements

The included published papers were reproduced with the permission of the journal of Applied Clay Science and The Clay Minerals Society (also thank you for putting one of my figures on the journal front page).

Tack till:

Staffan Hansen, för att under lång tid, med stor uthållighet och noggrannhet på ett mycket bra sätt handlett mitt doktorsarbete.

Anders Sjöland och Mats Ohlsson för att ni anställde mig på SKB och gav mig förtroendet och möjligheten att bli industridoktorand, och på olika vis stöttat mig.

Ola Karnland för att du som biträdande handledare givit värdefulla ramar, insikter och inriktningar och försökt se till att jag inte gjort allt för många eller stora misstag.

Patrik Sellin för att du tidigt släppte in mig i SKBs aktiva bentonitverksamhet, gett mig stort stöd i min utveckling, visat mig runt i världen och gett mig många bra råd och kontakter.

Alla mina chefer under årens lopp för att ha stöttat mig på ett mycket bra sätt i min utveckling och verksamhet. Alla kollegor på SKB, Claytech och Kemicentrum för all hjälp, vänlighet och trivsamhet. Speciellt tack till Christel Lundgren, Terese Bladström, Martin Birgersson, Magnus Hedström och Siv Olsson för all värdefull hjälp och givande diskussioner.

Many thanks to Joseph Stucki for a great visit to your lab, to Mark Raven for helping me out with the Siroquant software, and to Reiner Dohrmann, Stephan Kaufhold and George Christidis for great discussions.

Tack till Thomas Österberg och Jan-Olov Bovin för att på många sätt ha uppmuntrat mitt mineralintresse. Ett intresse som låg till grunden för detta arbete. Jag vill också tacka alla andra gamla goda vänner Linus, Daniel, Björn, Willy, och Mackan, som trots att tiden ofta varit knapp under dessa år ändå funnits kvar.

Sist men absolut inte minst, min älskade familj. Mina föräldrar som alltid stöttat mig och gett mig bästa möjliga förutsättningar. Min bror som sedan tidig ålder lärt mig en massa bra saker. Min kära Viktoria för att du alltid står vid min sida och att du stödjer mina platskrävande hobbys. Mina kära barn William och Linnea, tack för att ni finns ☺

References

Ahlrichs, J. L., White, J. L. (1962) Freezing and lyophilizing alters the structure of bentonite gels. *Science*, **136**, 1116-1118.

Åkesson, M., Olsson, S., Dueck, A., Nilsson, U., Karnland, O. (2012) TBT-Hydro-mechanical and chemical/mineralogical characterizations. *Swedish Nuclear Fuel and Waste Management Co* (*SKB) Technical Report*, P-12-06, SKB, Stockholm.

Alexander, W.R., Milodowski, A.E., Pitty, A.F. (2011) Cyprus natural analogue project (CNAP). Phase III final report. *Posiva Oy Working Report*, WR-11-77, Helsinki, Finland.

Amorim, C.L.G., Lopesa, R.T., Barrosob, R.C., Queirozc, J.C., Alvesc, D.B., Perezd, C.A., Scheline H.R. (2007) Effect of clay–water interactions on clay swelling by X-ray diffraction. *Nuclear Instruments and Methods in Physics Research Section A: Accelerators, Spectrometers, Detectors and Associated Equipment,* **580**, 768–770.

Anderson, D. M., Hoekstra, P. (1965) Migration of interlamellar water during freezing and thawing of Wyoming bentonite. *Soil Science Society of America Journal*, **29**, 498-504.

Arthur, R., Apted, M., Stenhouse, M. (2005) Comment on the long-term chemical and mineralogical stability of the buffer. *Swedish Nuclear Power Inspectorate*, SKI Report 2005:9.

Atkins, P. W. (1998) Physical chemistry. Oxford University Press, Oxford, USA.

Barshad, I. (1952) Factors affecting the interlayer expansion of vermiculite and montmorillonite with organic substances. *Proceedings Soil Science Society of America*, **16**, 176-182.

Bath, A. Hermansson, H.-P. (2009) Biogeochemistry of redox at repository depth and implications for the canister. Swedish Radiation Safety Authority, Report 2009:28.

Belyayeva, N. I. (1967) Rapid method for the simultaneous determination of the exchange capacity and content of exchangeable cations in solonetzic soils. *Soviet Soil Science*, **3**, 1409–1413.

Benson, H. (1995) University physics. John Wiley & Sons, USA.

Bergaya, F., Theng, B.K.G., Lagaly, G. (2006) Handbook of clay science. Developments in clay science, Volume 1, Elsevier Science, 1246 pp.

Birgersson, M. Karnland, O. (2009) Ion equilibrium between montmorillonite interlayer space and an external solution – consequences for diffusional transport. *Geochimica et Cosmochimica Acta*, **73**, 1908–1923.

Birgersson, M., Karnland, O., Nilsson, U. (2008) Freezing in saturated bentonite – A thermodynamic approach. *Physics and Chemistry of the Earth, Parts A/B/C*, **33**, 527-S530, Clays in Natural & Engineered Barriers for Radioactive Waste Confinement.

Brindley G. W., Brown G. (1980) Crystal structures of clay minerals and their x-ray identification. Mineralogical Society Monograph No. 5.

Brindley, G. W., Wiewiora, K., Wiewiora, A. (1969) Intracrystalline swelling of montmorillonite in some water-organic mixtures (Clay organic studies XVII). *American Mineralogist*, **54**, 1635-1644.

Carlson, S., Clausén, M., Gridneva, L., Sommarin, B., Svensson, C. (2006) XAFS experiments at beamline I811, MAX-lab synchrotron source, Sweden. *Journal of Synchrotron Radiation,* **13**, 359-364.

Carlson, L., Karnland, O., Oversby, V.M., Rance, A.P., Smart, N.R., Snellman, M., Vähänen, M., Werme, L.O. (2007) Experimental studies of the interactions between anaerobically corroding iron and bentonite. *Physics and Chemistry of the Earth,* **32**, 334-345.

Cerenius, Y., Ståhl, K., Svensson, L. A., Ursby, T., Oskarsson, Å. Albertsson, J., Liljas, A. (2000) The crystallography beamline I711 at MAX II, *Journal of Synchrotron Radiation*, 7, 203-208.

Charpentier, D., Devineau, K., Mosser-Ruck, R., Cathelineau, M., Villiéras, F. (2006) Bentonite-iron interactions under alkaline condition: An experimental approach. *Applied Clay Science,* **32**, 1-13.

Christidis, G. E., Eberl, D. D. (2003) Determination of layer-charge characteristics of smectites. *Clays and Clay Minerals*, **51**, 644-655.

Číčel, B., Novák, L, Horváth, L (1981) Mineralógia akryštalochémiaílov (The mineralogy and crystal chemistry of clays) VEDA, Publishing House of the Slovak Academy of Sciences, Bratislava.

Crank, J. (1980) The mathematics of diffusion, 2nd ed., Clarendon Press.

Delage, P., Marcial, D., Cui, Y. J., Ruiz, X. (2006) Ageing effects in a compacted bentonite: a microstructure approach. *Géotechnique*, **56**, 291-304.

Dueck, A., Johannesson, L. E., Kristensson, O., Olsson, S. (2011) Report on hydro-mechanical and chemical-mineralogical analyses of the bentonite buffer in Canister Retrieval Test. *Swedish Nuclear Fuel and Waste Management Co* (*SKB) Technical Report*, TR-11-07.

Eng, A., Nilsson, U., Svensson, D. (2007) Alternative Buffer Material – Installation report. *Swedish Nuclear Fuel and Waste Management Co* (*SKB) Report*, IPR-07-15.

Ferrage, E., Tournassat, C., Rinnert, E., Charlet, L., Lanson, B. (2005) Experimental evidence for Ca-chloride ion pairs in the interlayer of montmorillonite. An XRD profile modelling approach. *Clays and Clay Minerals*, **53**, 348-360.

Fisher, G. W. (1978) Rate laws in metamorphism. *Geochimica et Cosmochimica Acta*, **42**, 1035-1050.

Fukushima, Y. (1984) X-ray diffraction study of aqueous montmorillonite emulsions. *Clays and Clay Minerals*, **32**, 320-326.

Galoisy, L., Calas, G., Arrio, M.A. (2001) High-resolution XANES spectra of iron in minerals and glasses: structural information from the pre-edge region. *Chemical Geology,* **174**, 307-319.

Gorski, C. A., Klüpfel, L. E., Voegelin, A., Sander, M., Hofstetter, T. B. (2013) Redox properties of structural Fe in clay minerals: 3. Relationships between smectite redox and structural properties. *Environmental Science and Technology*, **47**, 13477-13485.

Grenthe, I., Stumm, W., Laaksuharju, M., Nilsson, A.-C., Wikberg, P. (1992) Redox potentials and redox reactions in deep groundwater systems. *Chemical Geology*, **98**, 131-150.

Guillaume, D., Neaman, A., Cathelineau, M., Mosser-Ruck, R., Peiffert, C., Abdelmoula, M., Dubessy, J., Villiéras, F., Michau, N. (2004) Experimental study of the transformation of smectite at 80 and 300 ºC in the presence of Fe oxides. *Clay Minerals,* **39**, 17-34.

Haneda, K., Morrish, A. H. (1977) Magnetite to maghemite transformation in ultrafine particles. *Journal de Physique Colloques*, **32**, C1-321-C1-323.

Hansen, E. L., Hemmen, H., Fonseca, D. M., Coutant, C., Knudsen, K. D., Plivelic, T. S., Bonn, D., Fossum, J. O. (2012) Swelling transition of a clay induced by heating. *Scientific Reports*, **2**, 618.

Hatharasinghe, H. L. M., Smalley, M. V., Swenson, J., Hannon, A. C., King, S. M. (2000) Freezing experiments on clay gels. *Langmuir*, **16** (13), 5562-5567.

Hedström, M. Karnland, O. (2011) Donnan equilibrium in Na-montmorillonite from a molecular dynamics perspective. *Geochimica et Cosmochimica Acta*, 77, 266-274.

Holmboe, M., Wold, S., Jonsson, M. (2012) Porosity investigation of compacted bentonite using XRD profile modeling. *Journal of Contaminant Hydrology*, **128**, 19-32.

Hover, V. C., Walter, L., M., Peacor, D. R., Martini, A. M. (1999) Mg-smectite authigenesis in marine evaporative environment, Salina Ometepec, Baja California. *Clays and Clay Minerals*, **47**, 252-268.

Jansson, M. (2009) Bentonite erosion – laboratory studies. *Swedish Nuclear Fuel and Waste Management Co* (*SKB) Technical Report*, TR-09-33.

Jönsson, B., Åkesson, T., Jönsson, B., Segad, M., Janiak, J., Wallenberg, R. (2009) Structure and forces in bentonite MX-80. *Swedish Nuclear Fuel and Waste Management Co* (*SKB) Technical Report*, TR-09-06.

Karnland, O., Birgersson, M. (2006) Montmorillonite stability – With special respect to KBS-3 conditions. *Swedish Nuclear Fuel and Waste Management Co* (*SKB) Technical Report*, TR-06-11.

Karnland O., Muurinen A., Karlsson F. (2005) Bentonite swelling pressure in NaCl solutions – Experimentally determined data and model calculations. Advances in Understanding Engineered Clay Barriers – Alonso, E.E. & Ledesma, A. (eds.), Taylor & Francis Group, London, 241-256.

Karnland, O., Olsson, S., Dueck, A., Birgersson, B., Nilsson, U., Hernan-Håkansson, T., Pedersen, K., Nilsson, S., Eriksen, T. E., Rosborg, B. (2009) Long term test of buffer material at the Äspö Hard Rock Laboratory, LOT project. Final report on the A2 test parcel. *Swedish Nuclear Fuel and Waste Management Co* (*SKB) Technical Report*, TR-09-29.

Karnland, O., Olsson, S., Nilsson, U. (2006) Mineralogy and sealing properties of various bentonites and smectite-rich clay material. *Swedish Nuclear Fuel and Waste Management Co* (*SKB) Technical Report*, TR-06-30.

Kaufhold, S., Dohrmann, R., Sandén, T., Sellin, P., Svensson, D. (2013) Mineralogical investigations of the alternative buffer material test – I. Alteration of bentonites. *Clay Minerals*, **48**, 199-213.

Kell, G.S. (1967) Volume properties of ordinary water. Journal of Chemical and Engineering Data, **12**, 67—68.

Keller, L. M., Holzer, L., Gasser, P., Erni, R., Rossell, M. D. (2014) Intergranular pore space evolution in MX80 bentonite during a long-term experiment. *Applied Clay Science*, accepted for publication 19 November 2014.

Kjellander, R., Marčelja, S., Pashley, R. M., Quirk, J. P. (1988) Double-layer ion correlation forces restrict calcium-clay swelling. *Journal of Physical Chemistry*, **92**, 6489-6492.

Klein, C., Hurlbut, C. S. (1998) Manual of mineralogy. 21st ed., John Wiley & Sons.

Kodama H. (1966) The nature of the component layers in rectorite. *American Mineralogist* **51**(7), 1035-1055.

Kuchta, L., Fajnor, V. S. (1987) Optimal conditions for hydrothermal synthesis of saponite. *Chemical Papers*, **42**, 339-345.

Kumpulainen, S., Kiviranta, L., Carlsson, T., Muurinen, A., Svensson, D., Sasamoto, H., Wersin, P. (2010) Long-term alteration of bentonite in the presence of metallic iron. SKB Report, R-10-52, SKB, Stockholm.

Kwiatek, W. M., Galka, M., Hanson, A. L., Paluszkiewicz, C., Cichocki, T. (2001) XANES as a tool for iron oxidation state determination in tissues. *Journal of Alloys and Compounds*, **328**, 276-282.

Lagaly, G. (1979) The "layer charge" of regular interstratified 2:1 clay minerals. *Clays and Clay Minerals*, **27**, 1-10

Lagaly, G. (1994) Layer charge determinations by alkylammonium ions. In: Mermut, A. (Ed.), Charge characteristics of 2:1 clay minerals. CMS Workshop lectures, vol 6. The Clay Minerals Society, Boulder, CO, 1-46.

Laird, D. A. (2006) Influence of layer charge on swelling of smectites. *Applied Clay Science*, **34**, 74-87.

Lantenois, S., Lanson, B., Muller, F., Bauer, A., Jullien, M., Plancon, A. (2005) Experimental study of smectite interaction with metal Fe at low temperature: 1. Smectite destabilization. *Clays and Clay Minerals*, **53**, 597-612.

Liu, D., Dong, H., Bishop, M.E., Zhang, J., Wang, H., Xie, S., Wang, S., Huang, L., Eberl, D. D. (2012) Microbial reduction of structural iron in interstratified illite-smectite minerals by a sulfate-reducing bacterium. *Geobiology*, **10**, 150-162.

Liu, J., Neretnieks, I. (2006) Physical and chemical stability of the bentonite buffer. *Swedish Nuclear Fuel and Waste Management Co* (*SKB) Report*, R-06-103.

Lucas, R. (1918) Ueber das Zeitgesetz des Kapillaren Aufsteigs von Flüssigkeiten. *Kolloid- Zeitschrift*, **23**, 15-22.

Mammen, C.B., Ursby,T., Cerenius, Y., Thunnissen, M., Als-Nielsen,J., Larsen, S., Liljas, A. (2002) Design of a 5-station macromolecular crystallography beamline at MAX-lab, *Acta Physica Polonica A*, **101**, 595.

Mammen, C.B., Ursby,T., Cerenius, Y., Thunnissen, M., Als-Nielsen,J. (2004) Bent Diamond Crystals and Multilayer Based Optics at the new 5-station protein crystallography beamline `Cassiopeia' at MAX-lab, AIP Conference Proceedings, 705, 808-811.

Marcus, Y. (1994) A simple empirical model describing the thermodynamics of hydration of ions of widely varying charges, sizes and shapes. *Biophysical Chemistry*, **51**, 111-127.

McKinstry, H. A. (1965) Thermal expansion of clay minerals. *American Mineralogist*, **50**, 212-222.

Mehra, O. P., Jackson, M. L. (1958) Iron oxide removal from soils and clays by a dithionite citrate system buffered with sodium bicarbonate. *Clays and Clay Minerals,* 7, 317-327.

Meier, L. P., Kahr, G. (1999) Determination of the cation exchange capacity (CEC) of clay minerals using complexes of copper(II) ion with triethylenetetramine and tetraethylenepentamine. *Clays and Clay Minerals*, **47**, 386-388.

Moore, D. M., Reynolds, R. C. (1997) X-ray diffraction and the identification and analysis of clay minerals. Oxford University Press.

Morillon, V., Debeaufort, F., Jose, J., Tharrault, J.F, Capelle,M., Blond, G., Voilley, A. (1999) Water vapour pressure above saturated salt solutions at low temperatures. *Fluid Phase Equilibria*, **155**, 297-309

Mosser-Ruck, R., Cathelineau, M., Guillaume, D., Charpentier, D., Rousset, D., Barres, O., Michau, N. (2010) Effects of temperature, pH, and iron/clay and liquid/clay ratios on experimental conversion of dioctahedral smectite to berthierine, chlorite, vermiculite, or saponite. *Clays and Clay Minerals*, **58**, 280-291.

Murad, E., Cashion, J. (2004) Mössbauer spectroscopy of environmental materials and their industrial utilization. Kluwer Academic Publishers, Norwell, Massachusetts, USA.

Norrish, K. (1954) The swelling of montmorillonite. *Discussions Faraday Society*, **18**, 120-134.

Norrish, K. Rausell-Colom, J. (1962) Effect of freezing on the swelling of clay minerals. *Clay Minerals Bulletin*, **5**, 9–16.

O'Day, P.A., Rivera Jr., N., Root, R., Carroll S.A. (2004) X-ray absorption spectroscopic study of Fe reference compounds for the analysis of natural sediments. *American Mineralogist*, **89**, 572-585.

Ogawa, M., Sato, T., Takahashi, N., Tanaka, M. (1991) Synthetic stevensite and process for preparation thereof. U.S. Patent 5,004,716 A, filed April 2, 1990, and published April 2, 1991.

Olsson, S., Jensen, V., Johanesson, L. E., Hansen, E., Karnland, O., Kumpulainen, S., Kirivanta, L., Svensson, D., Hansen, S., Lindén, J. (2013) Prototype Repository - Hydromechanical, chemical and mineralogical characterization of the buffer and backfill material from the outer section of the Prototype Repository. *Swedish Nuclear Fuel and Waste Management Co* (*SKB) Technical Report*, TR-13-21

Owen, B. B., Miller, R. C., Milner, C. E., Cogan, H. L. (1961) The dielectric constant of water as a function of temperature and pressure. *Journal of Physical Chemistry*, **65**(11), 2065-2070.

Paris, E., Mottana, A., Mattias, P. (1991) Iron environment in a montmorillonite from Gola del Furlo (Marche, Italy). A synchrotron radiation XANES and a Mössbauer study. *Mineralogy and Petrology*, **45**, 105-117.

Patterson, A. L. (1939) The Scherrer formula for x-ray particle size determination. *Physical Review*, **56**, 978-982.

Pentráková, L., Su, K., Pentrák, M., Stucki, J. W. (2013) A review of microbial redox interactions with structural Fe in clay minerals. *Clay Minerals*, **48**, 543-560.

Perronnet, M., Jullien, M., Villiéras, F., Raynal, J., Bonnin, D., Bruno, G. (2008) Evidence of a critical content in Fe(0) on FoCa7 bentonite reactivity at 80 °C. *Applied Clay Science*, **38**, 187-202.

Pusch, R. (2001) The buffer and backfill handbook. Part 2: Materials and techniques. *Swedish Nuclear Fuel and Waste Management Co* (*SKB) Technical Report*, TR-02-12.

Pusch, R., Madsen, F. T. (1995) Aspects on the illitization of the Kinnekulle bentonites. *Clays and Clay Minerals*, **43**, 261-270.

Pusch, R., Yong, R. (2003) Water saturation and retention of hydrophilic clay – buffer – microstructural aspects. *Applied Clay Science*, **23**, 61-68.

Quartieri, S., Riccardi, M.P., Messiga, B., Boscherini, F. (2005) The ancient glass production of the medieval Val Gargassa glasshouse: Fe and Mn XANES study. *Journal of Non-Crystalline Solids*, **351**, 3013-3022.

Rosborg, B. (2013) Recorded corrosion rates on copper electrodes in the Prototype Repository at the Äspö HRL. *Swedish Nuclear Fuel and Waste Management Co* (*SKB) Technical Report*, R-13-13.

Sandén, T., Goudarzi, R., Combarieu, M. Åkesson, M., Hökmark, H. (2007) Temperature buffer test – design, instrumentation and measurements. *Physics and Chemistry of the Earth*, **32**, 77-92.

Schnewberger, R., Voilley, A., Weisser, H. (1978) Activity of water in frozen systems. *International Journal of Refrigeration* **1**, 201–206.

Segad, M., Jönsson, B., Åkesson, T., Cabane, B. (2010) Ca/Na montmorillonite: structure, forces and swelling properties. *Langmuir*, **26** (8), 5782-5790.

SKB (2006) Long-term safety for KBS-3 repositories at Forsmark and Laxemar – a first evaluation. Main report of the SR-can project, *Swedish Nuclear Fuel and Waste Management Co* (*SKB) Technical Report*, TR-06-09.

SKB (2011) Redovisning av säkerhet efter förslutning av slutförvaret för använt kärnbränsle. Huvudrapport från projekt SR-Site, *Swedish Nuclear Fuel and Waste Management Co* (*SKB) report*.

Slade, P. G., Quirk, J. P., Norrish, K. (1991) Crystalline swelling of smectite samples in concentrated NaCl solutions in relation to layer charge. *Clays and Clay Minerals*, **39**, 234-238.

Sposito, G., Holtzclaw, K. M., Charlet, L., Jouany, C., Page, A. L. (1983) Sodium-calcium and sodium-magnesium exchange on Wyoming bentonite in perchlorate and chloride ionic media. *Soil Science Society of America Journal*, **47**, 51-56.

Stucki, J. W., Lee, K., Zhang, L., Larson, R. A. (2002) Effects of iron oxidation state on the surface and structural properties of smectites. *Pure and Applied Chemistry*, **74**, 2081-2094.

Stucki, J. W., Low, P. F., Roth, C. B., Golden, D. C. (1984) Effects of oxidation state of octahedral iron on clay swelling. *Clays and Clay Minerals*, **32**, 357-362.

Suquet, H., De La Calle, C., Pezerat, H. (1975) Swelling and structural organization of saponite. *Clays and Clay Minerals*, **23**, 1-9.

Suzuki, M., Wada, N., Hines, D. R., Whittingham, M. S. (1987) Hydration states and phase transitions in vermiculite intercalation compounds. *Physical Review B*, **36**, 2844-2851.

Svemar, C., Christiansson, R., Grahm, P., Hagman, P., Svensson, D., Johannesson, L. E., Kristensson, O., Lönnqvist, M., Malmberg, D., Nilsson, U., Wieczorek, K. (2013) Prototype Repository - Opening and retrieval of the outer section of the Prototype Repository at Äspö Hard Rock Laboratory. Summary Report. *Swedish Nuclear Fuel and Waste Management Co* (*SKB) Technical Report*, TR-13-22.

Svensson, D. (2013) Early observations in a large scale 6½ year iron-bentonite field experiment (ABM2) at Äspö hard rock laboratory, Sweden. Conference abstract, 50th annual meeting of Clay Mineralogical Society. October 6-10. Urbana-Champaign, Illinois, U.S.A.

Svensson, D., Dueck, A., Nilsson, U., Olsson, S., Sandén, T., Lydmark, S., Jägerwall, S., Pedersen, K., Hansen, S. (2011) Alternative buffer material. Status of the ongoing laboratory investigation of reference materials and test package 1. *Swedish Nuclear Fuel and Waste Management Co* (*SKB) Technical Report*, TR-11-06.

Svensson, P. D., Hansen, S. (2010a) Intercalation of smectite with liquid ethylene glycol - resolved in time and space by synchrotron X-ray diffraction. *Applied Clay Science*, **48**, 358-367.

Svensson, P. D., Hansen, S. (2010b) Freezing and thawing of montmorillonite - a time-resolved synchrotron X-ray diffraction study. *Applied Clay Science*, **49**, 127-134.

Svensson, P. D., Hansen, S. (2013a) Combined salt and temperature impact on montmorillonite hydration. *Clays and Clay Minerals*, **61**, 328-341.

Svensson, P. D., Hansen, S. (2013b) Redox chemistry in two iron-bentonite field experiments at Äspö hard rock laboratory, Sweden: an XRD and Fe K-edge XANES study. *Clays and Clay Minerals*, **61**, 566-579.

Svensson, P. D., Hansen, S. (2014) Formation of four-water-layer hydrates in divalent cation exchanged smectites. *Manuscript*.

Vogels, R.J.M.J., Kloprogge, J.T., Geus, J.W., Beers, A.W.F. (2005) Synthesis and characterization of saponite clays: Part 2. Thermal stability. *American Mineralogist*, **90**, 945-953.

Washburn, E.W. (1921) The dynamics of capillary flow. *Physical Review*, **17**, 273-283.

Wersin, P., Birgersson, M., Olsson, S., Karnland, O., and Snellman, M. (2008) Impact of corrosion-derived iron on the bentonite buffer within the KBS-3H disposal concept. The Olkiluoto site as case study. SKB Report, R-08-34, SKB, Stockholm.

White, A.F.,Yee, A. (1985) Aqueous oxidation-reduction kinetics associated with coupled electron-cation transfer from iron-containing silicates at 25 °C. *Geochimica et Cosmochimica Acta,* **49**, 1263-1275.

Wilke, M., Farges, F., Petit, P.-E., Brown Jr., G.E., Martin, F. (2001) Oxidation state and coordination of Fe in minerals: An Fe K-XANES spectroscopic study. *American Mineralogist*, **86**, 714-730.

Wilke, M., Partzsch, G.M., Bernhardt, R., Lattard, D. (2005) Determination of the iron oxidation state in basaltic glasses using XANES at the K-edge. *Chemical Geology* **220**, 143-161.

Wilson, J., Savage, D., Cuadros, J., Shibata, M., Ragnarsdottir, K. V. (2006) The effect of iron on montmorillonite stability. (I) Background and thermodynamic considerations. Geochimica et Cosmochimica Acta, **70**, 306-322.

Wu, J., Low, P. F., Roth, C. B. (1989) Effects of octahedral-iron reduction and swelling pressure on interlayer distances in Na-nontronite. *Clays and Clay Minerals*, **37**, 211-218.

Zavitsas, A. A. (2005) Aqueous solutions of calcium ions: Hydration numbers and the effect of temperature. *The Journal of Physical Chemistry B*, **109**, 20636-20640

Zhang, F., Zhang, Z. Z., Low, P. F., Roth, C. B. (1993) The effect of temperature on the swelling of montmorillonite. *Clay Minerals*, **28**, 23-31.

Zhang., G., Kim, J., Dong, H., Sommer, A. J. (2007) Microbial effects in promoting the smectite to illite reaction: Role of organic matter intercalated in the interlayer. *American Mineralogist*, **92**, 1401-1410.

Zhang, J., Hailiang, D., Liu, D., Agrawal, A. (2013) Microbial reduction of Fe(III) in smectite minerals by thermophilic methanogen Methanothermobacter thermautotrophicus. *Geochimica et Cosmochimica Acta*, **106**, 203-215.

Publications and manuscripts